Articles

Design, Synthesis, and X-ray Crystal Structure of a Potent Dual Inhibitor of Thymidylate Synthase and Dihydrofolate Reductase as an Antitumor Agent[1]

Aleem Gangjee,*,† Jianming Yu,† John J. McGuire,‡ Vivian Cody,§ Nikolai Galitsky,§ Roy L. Kisliuk,⊥ and Sherry F. Queener#

Division of Medicinal Chemistry, Graduate School of Pharmaceutical Sciences, Duquesne University, Pittsburgh, Pennsylvania 15282; Grace Cancer Drug Center, Roswell Park Cancer Institute, Elm and Carlton Streets, Buffalo, New York 14263; Hauptman−Woodward Medical Research Institute, Inc., 73 High Street, Buffalo, New York 14203; Department of Biochemistry, Tufts University School of Medicine, Boston, Massachusetts 02111; and Department of Pharmacology and Toxicology, School of Medicine, Indiana University, Indianapolis, Indiana 46202

Received May 9, 2000

A novel *N*-{2-amino-4-methyl[(pyrrolo[2,3-*d*]pyrimidin-5-yl)ethyl]benzoyl}-L-glutamic acid **(3a)** was designed and synthesized as a potent dual inhibitor of thymidylate synthase (TS) and dihydrofolate reductase (DHFR) and as an antitumor agent. Compound **3b**, the N7-benzylated analogue of **3a**, was also synthesized as an antitumor agent. The synthesis of **3a** was accomplished via a 12-step sequence which involved the synthesis of 2-amino-4-methylpyrrolo-[2,3-*d*]pyrimidine **(10)** in 5 steps from 2-acetylbutyrolactone. Protection of the 2-amino group of **10** and regioselective iodination at the 5-position followed by palladium-catalyzed coupling afforded intermediate **14** which was converted to **3a** by reduction and saponification. Similar synthetic methodology was used for **3b**. X-ray crystal structure of the ternary complex of **3a**, DHFR, and NADPH showed that the pyrrolo[2,3-*d*]pyrimidine ring binds in a "2,4-diamino mode" in which the pyrrole nitrogen mimics the 4-amino moiety of 2,4-diaminopyrimidines. This is the first example of a classical pyrrolo[2,3-*d*]pyrimidine antifolate shown to have this alternate mode of binding to DHFR. Compounds **3a** and **3b** were more inhibitory than LY231514 against TS from *Lactobacillus casei* and *Escherichia coli*. Analogue **3a** was also more inhibitory against DHFR from human, *Toxoplasma gondii*, and *Pneumocystis carinii*. Evaluation of **3a** against methotrexate (MTX)-resistant cell lines with defined mechanisms indicated that cross-resistance of **3a** was much lower than that of MTX. Metabolite protection studies and folylpoly-γ-glutamate synthetase studies suggest that the antitumor activity of **3a** against the growth of tumor cells in culture is a result of dual inhibition of TS and DHFR. Compound **3a** inhibited the growth of CCRF-CEM and FaDu cells in culture at ED_{50} values of 12.5 and 7.0 nM, respectively, and was more active against FaDu cells than MTX. In contrast, compound **3b** was inactive against both cell lines. Compound **3a** was evaluated in the National Cancer Institute in vitro preclinical antitumor screening program and afforded IG_{50} values in the nanomolar range against a number of tumor cell lines.

Introduction

Inhibitors of folate metabolism have provided important agents useful in cancer chemotherapy as a result of their inhibition of the biosynthesis of nucleic acid precursors.[2,3] The cofactor tetrahydrofolate (THF) is formed by the NADPH-dependent reduction of 7,8-dihydrofolate (7,8-DHF) by the enzyme dihydrofolate reductase (DHFR)[4] and serves as the principal component in folate metabolism as a carrier of one-carbon units in its various cofactor forms.[5] The synthesis of deoxythymidylate (dTMP) from deoxyuridylate (dUMP) is catalyzed by thymidylate synthase (TS) and utilizes 5,10-methylenetetrahydrofolate as the source of the methyl group of dTMP as well as the reductant.[6] This reaction affords 7,8-DHF which needs to be reduced by DHFR to THF. Thus TS coupled with DHFR forms a crucial link responsible for the synthesis of dTMP and hence DNA. Inhibitors of TS derived from substrate analogues such as 5-fluorouracil[7] and from folate analogues such as ZD1694 (Tomudex)[8] (Chart 1) have found utility as clinically important antitumor agents. Similarly the DHFR inhibitor methotrexate (MTX) is a mainstay in single and combination cancer chemotherapy.[9] Several TS and DHFR inhibitors which are analogues of folate have also shown antitumor activities in vitro and in vivo with some currently in clinical trials.[10,11]

* To whom correspondence should be addressed. Phone: 412-396-6070. Fax: 412-396-5593. E-mail: gangjee@duq.edu.
† Duquesne University.
‡ Roswell Park Cancer Institute.
§ Hauptman−Woodward Medical Research Institute, Inc.
⊥ Tufts University School of Medicine.
Indiana University.

10.1021/jm000200l CCC: $19.00
Published on Web 09/13/2000

Chart 1

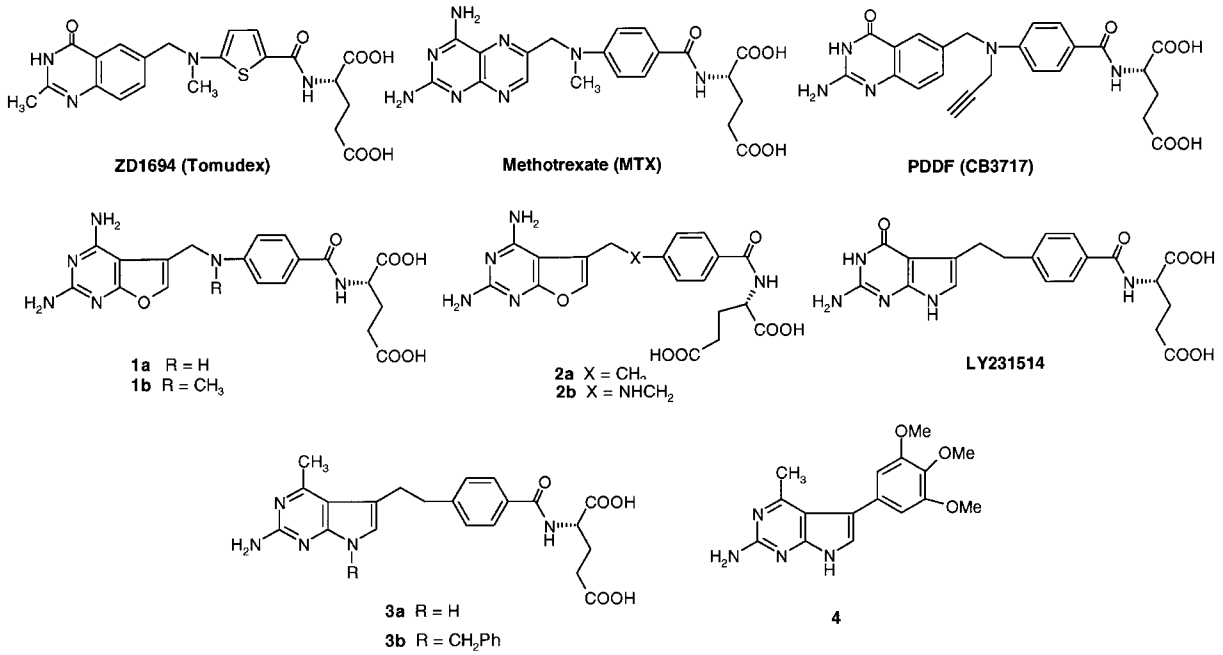

Folate analogues which inhibit TS generally contain a 2-amino-4-oxo or 2-methyl-4-oxo substitution in the pyrimidine ring of the antifolate.[12,13] Important examples of the former and latter analogues are N^{10}-propargyl-5,8-dideazafolate (CB3717, PDDF)[14] and ZD1694,[8] respectively. In contrast, inhibitiors of DHFR generally contain a 2,4-diamino substitution in the pyrimidine ring,[12,13] as exemplified by MTX.

It has been demonstrated, both in clinically available agents as well as in experimental agents, that TS inhibitors and DHFR inhibitors when used separately or in combination with other agents can provide successful antitumor therapy. In addition, synergism of two separate antifolates which inhibit TS and DHFR has been demonstrated in growth inhibitory studies against *Lactobacillus casei*,[15,16] rat hepatoma cells,[17,18] and human lymphoma cells.[15,19,20] Thus one of the goals of our efforts has been to design dual TS and DHFR inhibitory activity in a single agent. Such dual inhibitors could act at two different sites (TS and DHFR) and might be capable of providing "combination therapy" in a single agent without the pharmacokinetic disadvantages of two separate agents. 2,4-Diaminoquinazoline analogues as dual inhibitors were reported by Hynes et al.[21] with the suggestion that chemotherapeutic utility of such analogues would require that the inhibitory activity against DHFR be similar to that against TS.

Our initial effort toward the synthesis of dual DHFR−TS inhibitors involved the synthesis of 6-5 fused classical 2,4-diaminofuro[2,3-*d*]pyrimidines.[22,23] These novel 6-5 furo[2,3-*d*]pyrimidine compounds, *N*-[4-[*N*-[(2,4-diaminofuro[2,3-*d*]pyrimidin-5-yl)methyl]amino]benzoyl]-L-glutamic acid **(1a)**[22] and *N*-[4-[*N*-[(2,4-diaminofuro-[2,3-*d*]pyrimidin-5-yl)methyl]methylamino]benzoyl]-L-glutamic acid **(1b)**,[22] were designed to bind in the "2,4-diamino mode" (Figure 1) to DHFR and the "2-amino-4-oxo" mode to TS and hence function as dual inhibitors of DHFR and TS. Though compounds **1a** and **1b** were moderate inhibitors of DHFR from various sources (e.g., IC_{50} human DHFR 0.45 and 0.22 μM for **1a** and **1b**, respectively), in general the compounds were poor inhibitors of TS (IC_{50} human TS >200 μM for both **1a** and **1b**). In addition **1a** and **1b** were inactive against both glycinamide ribonucleotide formyltransferase (GARFT) and 5-aminoimidazole-4-carboxamide ribonucleotide formyltransferase (AICARFT). However both analogues were potent inhibitors of the growth of human T-lymphoblastic leukemia cell line CCRF-CEM in culture (EC_{50} 142 and 47 nM for **1a** and **1b**, respectively) and the growth of human squamous cell carcinoma FaDu in culture (ED_{50}[22] 126 and 55 nM for **1a** and **1b**, respectively), in continuous exposure. These analogues were efficiently polyglutamylated by human folylpoly-γ-glutamate synthetase (FPGS). These results suggested that polyglutamylation plays a role in their cellular mechanism of action. Thus it appeared that though **1a** and **1b** did not inhibit isolated TS to any significant extent, their polyglutamylated forms could be potent inhibitors of TS in tumor cells in culture, and hence compounds **1a** and **1b** were likely dual inhibitors of DHFR and TS. Metabolite protection studies however indicated that the mechanism of action of inhibition of tumor cells in culture for **1a** and **1b** was not the result of dual inhibition of DHFR and TS.[22] Analogues of **1a** and **1b** where the C8−N9 bridge was isosterically replaced by a C8−C9 bridge as in compound **2a**[23] and a C8−N9−C10 bridge as in compound **2b** gave much lower inhibition of tumor cells than **1a** and **1b**. Metabolite protection studies suggested that DHFR was the primary target of **2a** and **2b**. The compounds were poor inhibitors of TS as well as DHFR and moderately inhibited the growth of CCRF-CEM cells in culture (IC_{50} 0.25 μM for **2a** and 30.5 μM for **2b**).

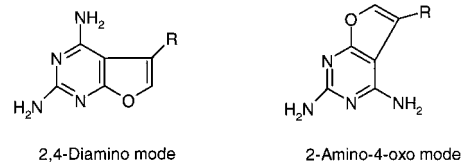

Figure 1. 2,4-Diaminofuro[2,3-*d*]pyrimidine.

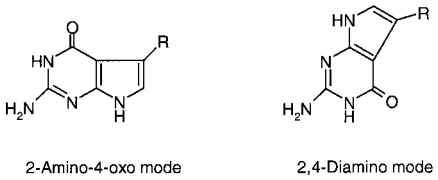

Figure 2. 2-Amino-4-oxopyrrolo[2,3-*d*]pyrimidine.

LY231514, a 2-amino-4-oxo classical pyrrolo[2,3-*d*]-pyrimidine antifolate and a potent inhibitor of tumor cell growth is currently in phase II/III trials as an antitumor agent.[24] This compound has been designated as a multitargeted antifolate (MTA) and is reported to be a reasonable inhibitor of both isolated TS and DHFR: in its polyglutamate forms, the inhibition against TS increases by several orders of magnitude. Molecular modeling of LY231514 using SYBYL 6.3[25] and superimposing it on the crystal structures of human DHFR with MTX showed that if LY231514 binds in the 2,4-diamino mode (Figure 2) to DHFR such that the pyrrole N mimics the 4-amino group of MTX, by rotation of 180° about the NH_2−C2 bond, then the 4-oxo moiety of LY231514 interacts with Phe31 and Leu22 of DHFR. Despite this interaction, LY231514 is reported to be a good inhibitor of human DHFR. We reasoned that if the 4-oxo moiety of LY231514 were removed or, better, replaced by a methyl group, the interaction of the 4-oxo with the hydrophobic Phe31 and Leu22 of the enzyme would be replaced by a productive hydrophobic interaction of the 4-methyl, thus increasing the DHFR inhibitory potency. Replacement of the 4-oxo in LY231514 with a 4-methyl affords *N*-{2-amino-4-methyl[(pyrrolo-[2,3-*d*]pyrimidin-5-yl)ethyl]benzoyl}-L-glutamic acid (**3a**). It was anticipated that **3a** would bind to DHFR in the 2,4-diamino mode where the pyrrole nitrogen mimics the 4-amino of DHFR inhibitors such as MTX. In this mode of binding the 4-methyl group of **3a** was predicted to interact with the Phe31 and Leu22 of human DHFR to afford potent inhibition. In the 2,4-diamino mode, the pyrrolo nitrogen atom may hydrogen bond with the carbonyl of Val115 and Ile7 and the hydroxyl of Tyr121 in human DHFR. This alternate mode of binding of pyrrolo[2,3-*d*]pyrimidines was first suggested by Miwa et al.,[26] and recently Kuyper et al.[27] showed that the nonclassical antifolate 2-amino-4-methyl-5-(3′,4′,5′-trimethoxyphenyl)-7*H*-pyrrolo[2,3-*d*]pyrimidine (**4**) does bind to *Escherichia coli* DHFR in the 2,4-diamino mode where the pyrrole nitrogen mimics the 4-amino moiety of MTX and piritrexim (PTX). These reports lend further credence to the design of **3a** as a potent inhibitor of DHFR.

In addition to the inhibition of DHFR we were also interested in the inhibition of TS in an attempt to provide dual DHFR−TS inhibitors. Molecular modeling using SYBYL 6.3 (Figure 3) of **3a** in the crystal structure of CB3717 with *E. coli* TS[28] or Tomudex (ZD1694) and *E. coli* TS[29] with **3a** superimposed on each inhibitor (CB3717 or ZD1694), such that the pyrrole nitrogen is positioned on the 4-oxo moiety of CB3717 or ZD1694, showed that in this alignment the 4-methyl group mimics the quinazoline C8 of CB3717 and ZD1694 and can interact with Leu143 (3.42 Å) just as the C7 and C8 positions of the quinazolines do in CB3717 and ZD1694. The pyrrole nitrogen with its hydrogen mimics the 4-oxo moiety and interacts in a hydrogen bond with Asp169 and also makes contact with the 4C═O of dUMP and with Gly173. In addition the stacking interaction of the pyrrolo[2,3-*d*]pyrimidine in the 2,4-diamino mode of **3a** is more appropriately aligned with dUMP than either CB3717 or ZD1694. This stacking interaction was expected to provide additional binding for **3a** compared with CB3717 or ZD1694. We have used *E. coli* TS as a surrogate for human TS in our molecular modeling studies because a high-resolution human TS crystal structure is not currently available. The minor differences in the sequence of *E. coli* TS and human TS are His51, Trp83, and Val262 (*E. coli* TS) and Phe80, Asn112, and Met311 (human TS). In addition, Webber et al.,[30] Appelt et al.,[31] Varney et al.,[32] and Reich et al.[33] have utilized the crystal structure of *E. coli* TS as a surrogate for human TS in molecular modeling studies which afforded potent human TS inhibitors and a clinically active antitumor agent in the case of AG337[30] which is in phase II/III trials.

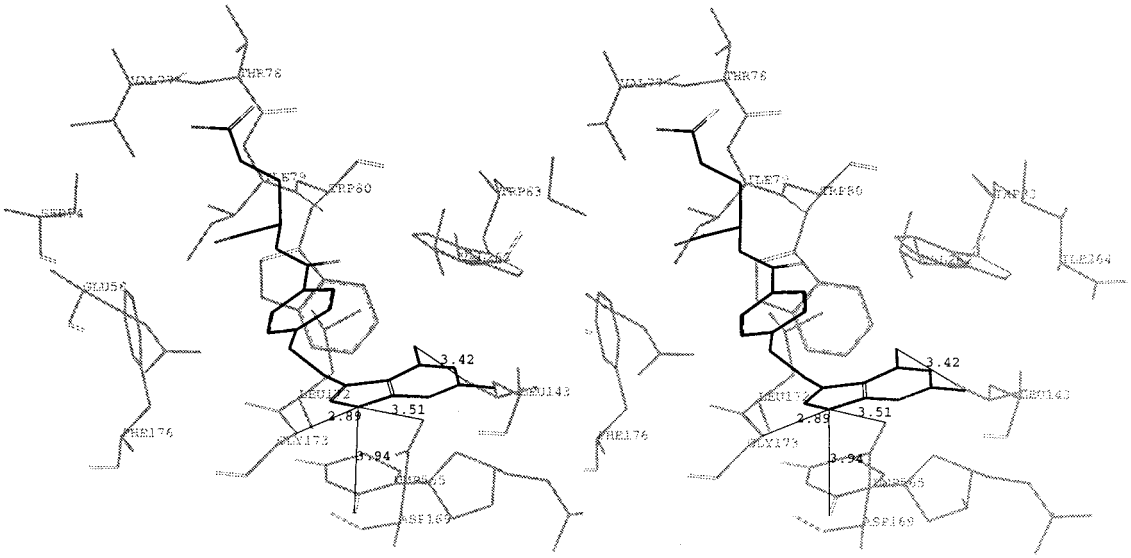

Figure 3. Compound **3a** superimposed on the crystal structure of ZD1694 (not shown) bound to *E. coli* TS and NADPH, showing contacts of the 4-Me and N7 of **3a** with residues of *E. coli* TS.

Thus, structural features which allow compound **3a** to function as a potent dual DHFR−TS inhibitor, without the necessity of undergoing polyglutamylation, were incorporated in the structure-based design of **3a**.

The antitumor activities of several classical antifolates, particularly TS inhibitors, are in part determined by their ability to function as substrates for the enzyme FPGS.[34−39] Polyglutamylation catalyzed by FPGS produces long-acting, noneffluxing poly-γ-glutamates of classical antifolates that lead to high intracellular concentrations of these antitumor agents. Further, polyglutamylation provides for a significant increase in inhibitory activity against TS compared to the monoglutamates.[34,35,37−40] It has been shown for both ZD1694[34] and LY231514[35] that the conversion of the monoglutamate form of these compounds to their pentaglutamates produces a 60-fold (for ZD1694) to 130-fold (for LY231514) increase in TS inhibition. Though polyglutamylation for many antifolates is necessary for cytotoxicity to tumor cells, it has also been implicated in adverse effects on normal tissues due to retention of poly-γ-glutamate metabolites.[37,41] The problem of resistance in tumors, which is a result of low or defective FPGS, is also a potential limitation of the use of such classical antifolates, which depend on polyglutamylation for their antitumor effects.[42−45]

Takeda Chemical Industries[46] claimed that a broad variety of 7-substituted derivatives (including a benzyl group) of LY231514 were active antitumor agents. In contrast, Taylor et al.[47] found that N-substitution at the 7-position of LY231514 eliminated cell growth inhibitory activity. It was therefore of interest to synthesize the N7-benzyl analogue of **3a**, to explore the effect of N7-substitution on biological activity. Thus, compound **3b** was also synthesized and evaluated.

Chemistry

The synthesis of the target compound **3a** was accomplished starting with the synthesis of the key intermediate 2-amino-4-methylpyrrolo[2,3-*d*]pyrimidine **(10)** (Scheme 1). A search of the literature revealed that

Scheme 1[a]

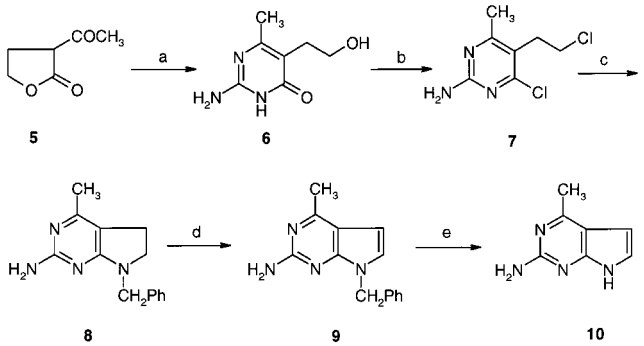

[a] Reagents: (a) guanidine carbonate, EtOH, triethylamine, reflux; (b) $POCl_3$, reflux; (c) benzylamine, triethylamine, *n*-BuOH, 90 °C; (d) MnO_2, 1,4-dioxane, reflux; (e) Na/liq NH_3, −78 °C.

there was no report for this compound. Our synthetic method was sparked by the recent report of Badaway[48] of several furo-, thieno-, and pyrrolo[2,3-*d*]pyrimidines from 2-acetylbutyrolactone **(5)**. This method was modified to afford a synthesis for the desired intermediate **10**. Compound **5** and guanidine carbonate were refluxed with absolute ethanol in the presence of triethylamine (method A) or sodium methoxide (method B) to afford **6** in 69% and 57% yield, respectively. Compound **6** was converted to **7** in 68% yield by refluxing with phosphorus oxychloride. Condensation of benzylamine with **7** in the presence of triethylamine under reflux in *n*-BuOH afforded the bicyclic compound **8** in 50% yield. Attempts to oxidize **8** to the aromatic compound **9** using reported methods (DDQ;[49] 10% Pd/C[50]) were unsuccessful. MnO_2,[51] however, afforded **9** in acceptable yield (45%).

The initial optimism resulting from the facile synthesis of **9** was diminished following numerous unfruitful attempts to remove the N7-benzyl protecting group to afford the pyrrolo[2,3-*d*]pyrimidine **10**. The N7-benzyl group could not be removed under a variety of conditions (e.g., Pd/C/H_2, 50 psi; Pd(OH)$_2$−C/$HCOONH_4$;[52] Pd−C/H_2/HCOOH; sodium naphthalene[53]). Changing the protecting group to a 2,4-dimethoxybenzyl moiety also resisted debenzylation conditions[54] (CF_3COOH;[55] CAN[56]). Finally, it was found that sodium in liquid ammonium at −78 °C[57] afforded the debenzylation of **9** to **10** in good yield (70%).

With intermediate **10** in hand, the 2-amino group was protected with pivaloyl chloride which both increased the solubility of **10** and, more importantly, directed the iodination regioselectively to the 5-position in the subsequent step (Scheme 2). Compound **12** was the sole

Scheme 2[a]

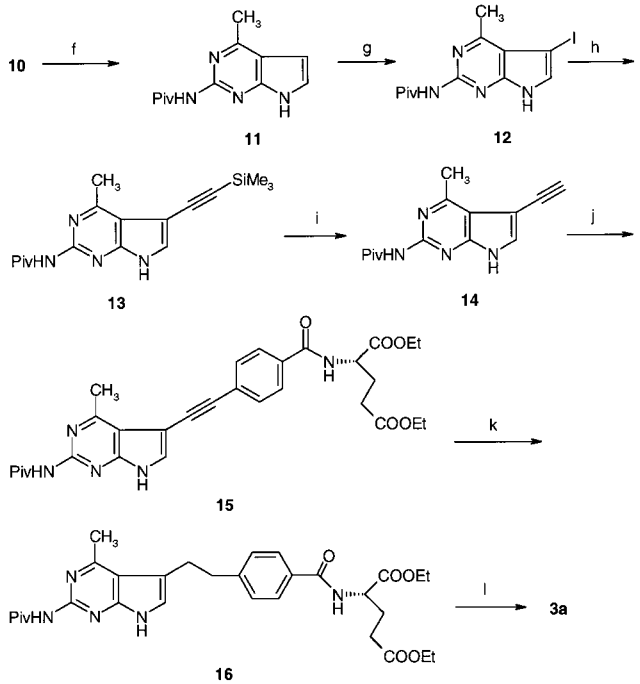

[a] Reagents: (f) PivCl, pyridine, reflux; (g) NIS, dark, rt; (h) trimethylsilylacetylene, CuI, tetrakis(triphenylphosphine)palladium(0), triethylamine, THF, rt; (i) *n*-Bu_4NF, THF, rt; (j) CuI, tetrakis(triphenylphosphine)palladium(0), diethyl 4-iodobenzoyl-L-glutamate, triethylamine, THF, rt; (k) 5% Pd/C, H_2, 50 psi; (l) 1 N NaOH, MeOH, 50 °C.

product obtained using NIS as the iodinating agent. The structure of **12** as a monoiodo derivative was established from its elemental analysis and ^{1}H NMR. Similar 2-pivaloylated 2-aminopyrrolo[2,3-*d*]pyrimidine analogues with 4-Cl, 4-OMe, and 4-oxo substituents have been reported in the literature.[58,59] In the unhalogenated

analogues the H6 is always found 0.50−1.00 ppm (6.95−7.51 ppm) deshielded compared to H5 (6.38−6.51 ppm). On iodination at C5, H6 occurs in the range of 7.12−7.74 ppm.[58,59] The ^{1}H NMR of **11** shows H5 and H6 at 6.65 and 7.35 ppm, respectively. Further, ^{1}H NMR of **12** indicated H6 at 7.71 ppm as a doublet (J = 2.2 Hz) due to coupling with the adjacent N7-H. The ^{1}H NMR along with the elemental analysis confirmed the structure of **12** and unequivocally established the 5-position as the site of iodination with NIS.

To directly afford diethyl *N*-{2-pivaloylamino-4-methyl[(pyrrolo[2,3-*d*]pyrimidin-5-yl)ethynyl]benzoyl}-L-glutamate **(15)**, the Sonogashira method[60] was attempted to couple **12** with diethyl 4-ethynylbenzoyl-L-glutamate, in the presence of tetrakis(triphenylphosphine)palladium(0) ($Pd(PPh_4)_3$), copper(I) iodide (CuI), and triethylamine in THF. This versatile methodology has been adopted with success by several groups;[58,61] however, it was unsuccessful in our hands under the reported conditions as well as with the use of different solvents (DMF, 1,2-dichloroethane, methylene chloride) or temperatures.

Attention was then turned to an alternate method to couple **12** with trimethylsilylacetylene under the same conditions ($Pd(PPh_4)_3$, CuI, triethylamine) in THF. This afforded **13** in 70% yield. The silyl protecting group of **13** was removed by fluoride ion to afford **14** in 90% yield. Compound **14** was then successfully coupled with diethyl 4-iodobenzoyl-L-glutamate, under palladium-catalyzed reaction conditions as adopted for **12** to **13**, to give **15** in 43% yield. Subsequent catalytic hydrogenation was accomplished with hydrogen and 5% palladium-on-charcoal in a mixture of methanol and methylene chloride (1:1) without reduction of the pyrrole ring. Treatment of the resulting ethano-bridged intermediate **16** with 1 N NaOH at 50 °C for 3 days resulted in simultaneous saponification of the ester functionalities and removal of the pivaloyl protecting group at 2-NH_2 to afford target compound **3a**.

For the synthesis of the N7-benzyl analogue **3b**, it was assumed that pivaloylation of **9** from Scheme 1 would afford the N7-benzyl analogue of **11** (Scheme 2) from which **3b** would be obtained as outlined in Scheme 2. However, iodination with NIS of the N7-benzyl analogue of **11** afforded several products, a majority of which was the 5,6-diiodo derivative. Ramzaeva and Seela[62] have suggested that regioselective halogenation of similar systems is controlled by the electron density of the pyrrole ring and that decreasing this density affords regioselective halogenation. Since a pivaloyl group was already present on the 2-NH_2, it was necessary to further decrease the electron density of the pyrrole ring. Thus the 2-NH_2 moiety was dipivaloylated from **9** as shown in Scheme 3 to afford **17**. Iodination of **17** with NIS afforded regioselectively the 5-iodo derivative **18** as the sole product. Compound **3b** was obtained from **18** following the procedure outlined for **3a**.

Scheme 3[a]

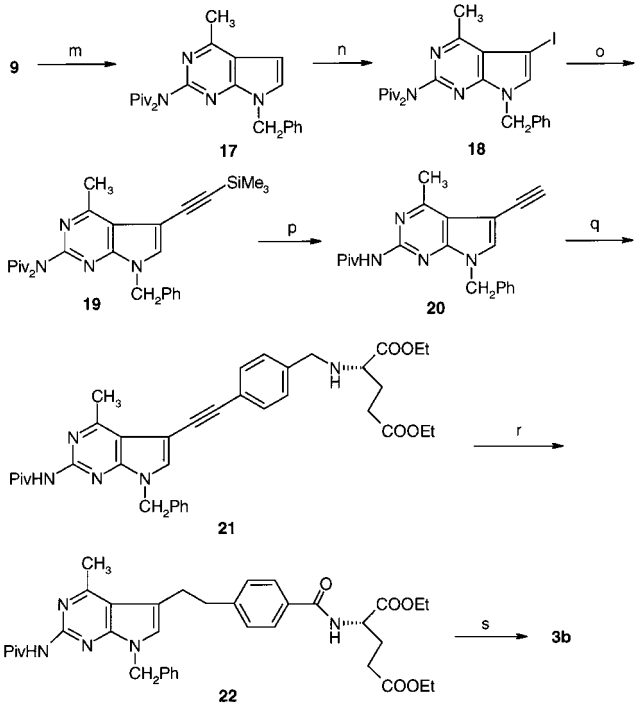

[a] Reagents: (m) PivCl, DMAP, triethylamine, dichloroethane, 50 °C; (n) NIS, DMF, dark, rt; (o) trimethylsilylacetylene, CuI, tetrakis(triphenylphosphine)palladium(0), triethylamine, THF, rt; (p) *n*-Bu_4NF, THF, rt; (q) CuI, tetrakis(triphenylphosphine)palladium(0), diethyl 4-iodobenzoyl-L-glutamate, triethylamine, THF, rt; (r) 5% Pd/C, H_2, 50 psi; (s) 1 N NaOH, MeOH, 50 °C.

X-ray Crystal Structure

The X-ray crystal structure of the ternary complex of **3a**, NADPH, and *Pneumocystis carinii* DHFR was determined. Careful analysis of the difference electron density maps (Figure 4) was carried out to validate the binding orientation of **3a**. When the inhibitor was placed in the orientation observed for the crystal structure of the classical 2,4-diaminofuro[2,3-*d*]pyrimidine analogues **1b**,[63] there was a break in the electron density between ring fragments and there was negative density in the putative N8 position. When the pyrrolo[2,3-*d*]-pyrimidine ring was flipped into the 2,4-diamino mode, there was continuous density for the molecule and no negative density, indicating that this model properly fit the observed data.

While the overall characteristics of the *P. carinii* DHFR ternary complex with NADPH and **3a** are similar to those reported for other *P. carinii* DHFR complexes,[63,64] the unusual feature of this ternary complex is that the pyrrole ring nitrogen N7 of **3a** interacts with the nicotinamide ring of NADPH and forms a single hydrogen bond with the carbonyl oxygen of the conserved Ile10. These data provide the first structural observation of a flipped orientation of the 2-amino-4-methylpyrrolo[2,3-*d*]pyrimidine ring system of a classical antifolate structure. As illustrated (Figure 5), the 4-methyl group occupies the pocket near Glu32, a position normally occupied by N8 of MTX or O4 of folate (FA). This binding is similar to that for the *E. coli* DHFR complex reported for the nonclassical pyrrolo[2,3-*d*]-pyrimidine complex.[27] The methyl group occupies a hydrophobic enviroment surrounded by the side chains of Leu25 and Ile33 (Leu22 and Phe31 in the human enzyme) and results in a small displacement of the conserved water molecule that forms the hydrogen-bonding network observed for nearly all DHFR crystal structures. The effect of the ethyl bridge (C9−C10) compared to the normal C9−N10 antifolate bridge is to change the electrostatics of this region of the active site.

Despite the binding with a flipped orientation, key enzyme interactions of **3a** are conserved. The carboxyl-

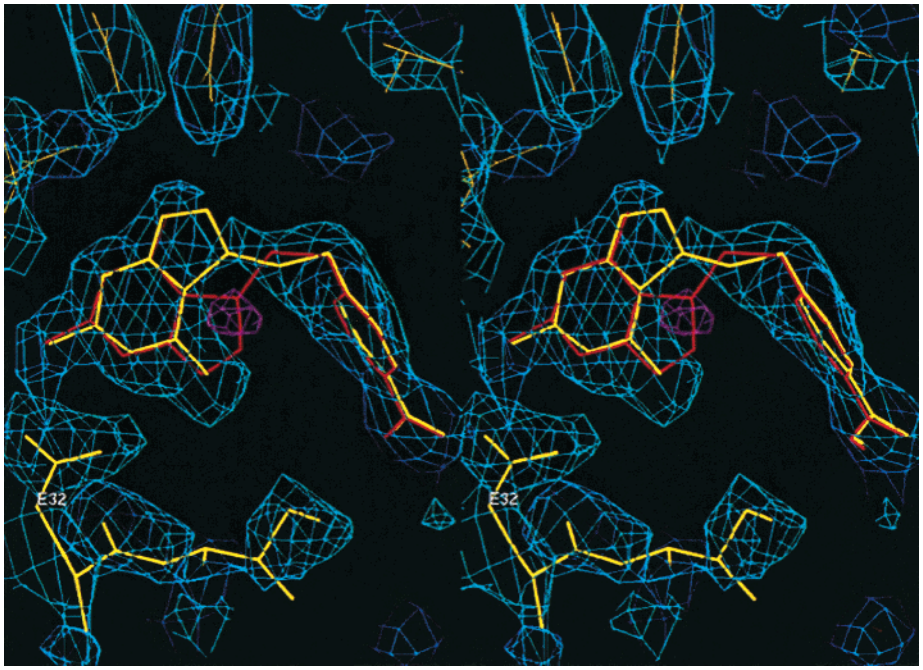

Figure 4. Stereoview of the electron density ($2F_o - F_c$, 1σ) (blue) for pcDHFR showing the fit of the inhibitor **3a** in the 2-amino-4-oxo mode (red), similar to that observed for the furo[2,3-*d*]pyrimidine classical antifolate **1b**, and in the 2,4-diamino mode (yellow), similar to that observed for the cyclized TMP derivative.[27] Note the break in the electron density between the pyrrolo ring system and the ethylene bridge system for the 2-amino-4-oxo mode. Also shown is the electron density ($F_o - F_c$, -3σ) (violet) showing that the mode does not fit the data in this orientation. There is no break in the electron density, nor is there negative density for the correct model, the 2,4-diamino mode. Model made from the program CHAIN.

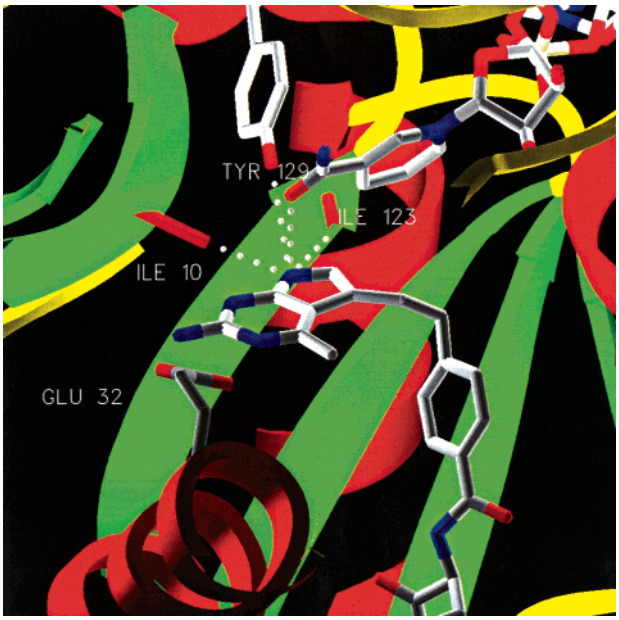

Figure 5. View highlighting the interaction of the pyrrole N7 of **3a** with the conserved residues Ile10, Ile123, and Tyr129 and the nicotinamide group of NADPH in the structure of the pcDHFR−NADPH−**3a** ternary complex. The helices are colored red, the sheets green, and the loops yellow. Hydrogen-bonded contacts are shown with white dashes. Model made with the SETOR program.

ate oxygens of Glu32 interact with the pyrrolo[2,3-*d*]-pyrimidine ring forming contacts with the N1 nitrogen by OE2 and OE2 to the 2-NH_2 nitrogen. In addition, the carboxylate oxygen OE1 of Glu32 forms a hydrogen bond to the hydroxyl of Thr144 which, in turn, interacts with a conserved water molecule and also with the 2-NH_2 group of **3a**. There is a further hydrogen-bonding network formed by another conserved water molecule which forms contacts with OE2 of Glu32 and NE2 of Trp27. Similar patterns have been observed in most DHFR crystal structures.[63,64]

Table 1. HB Contacts in DHFR−NADPH Inhibitor Complexes[a]

contacts	pc−**3a**	pc−MTX	pc−**1b**	h−**1b**	h−**3a** model
N8 or N7···I10 O	3.1	2.5	3.1	3.1	3.2
4-NH_2···I123 O	3.3	3.0	2.9	3.4	3.4
4-NH_2···Y129 OH	3.6	3.3	3.4	3.7	3.5
4-NH_2···nic O	3.1	3.6	2.7	3.6	2.9
4-CH_3···Wat	3.4				
N8···Wat		2.8			
O7···Wat				4.0	

[a] pc = *P. carinii*; h = human. Values given in Å.

The contacts of the pyrrole N7 in the *P. carinii* DHFR enzyme site are compared with those of the 4-amino substituent of other antifolates. As illustrated in Table 1, the 4-amino group of antifolates such as MTX and **1b** make a large number of close contacts to the surrounding hydrophilic conserved residues (i.e., Ile10, Ile123, Tyr129, and the nicotinamide keto function for *P. carinii* DHFR). These contacts are weaker in the human DHFR structures than for the *P. carinii* DHFR enzyme. The binding of **3a** in the active site of human DHFR was also modeled (Figure 6), and these results show no unexpected interactions (Table 1).

Analysis of these structures shows that the region near the nicotinamide ring requires a strong hydrogen-bonding partner to interact with the conserved Ile10 and Ile123 backbone carbonyl oxygens (*P. carinii* DHFR numbering). However, the region near the conserved acidic function, Glu32, is more flexible as it can readily

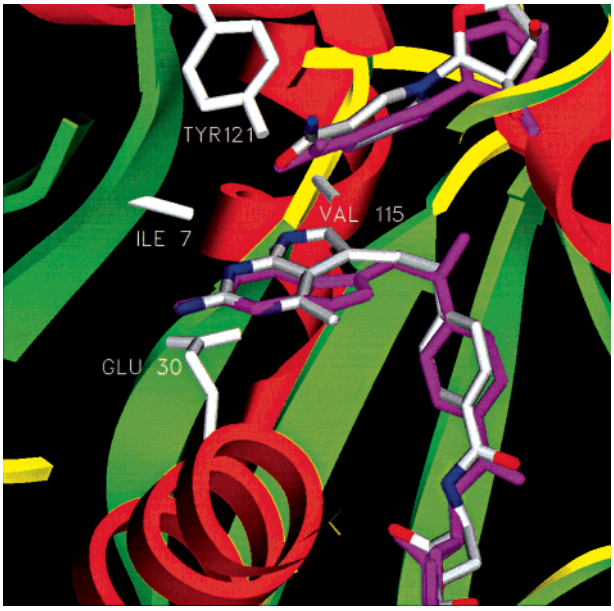

Figure 6. View comparing the interactions of the pyrrole N7 of **3a**, modeled in the active site of hDHFR, and that of the furo[2,3-*d*]pyrimidine antifolate **1b** with the conserved residues Ile7, Val115, and Tyr121 and the nicotinamide group of NADPH. Note that the Tyr121 no longer makes close contacts to the pyrrole N7. Model made with the SETOR program.

Table 2. Inhibitory Concentrations against Isolated TS

	IC_{50} (M)			
compd	*L. casei*	*E. coli*	rat	human[a]
3a	9.0×10^{-6}	2.0×10^{-6}	2.0×10^{-6}	1.0×10^{-6}
3b	3.1×10^{-7}	1.6×10^{-5}	$>1.6 \times 10^{-5}$	$>1.6 \times 10^{-5}$
LY231514[b]	2.0×10^{-5}	1.1×10^{-4}	2.0×10^{-5}	1.1×10^{-5}
ZD1694[c]	8.0×10^{-6}	1.0×10^{-5}	9.0×10^{-7}	1.0×10^{-6}
PDDF[d]	5.5×10^{-8}	1.0×10^{-7}	3.6×10^{-7}	1.5×10^{-7}

[a] Kindly provided by Dr. F. Maley, New York State Department of Health, Albany, NY. [b] Kindly provided by Dr. Chuan Shih, Eli Lilly & Co., Indianapolis, IN. [c] Kindly provided by Dr. Ann Jackman, Institute of Cancer Research, Sutton, Surrey, U.K. [d] Kindly provided by Dr. M. G. Nair, University of South Alabama, Mobile, AL.

accommodate such substitutents as N-H from MTX, O from folate or **1b**, and CH_3, as shown in this pyrrolo-[2,3-*d*]pyrimidine structure. Similar results were observed in the crystal structure complexes of human DHFR with the lipophilic antifolates 6-methyl-5-adamantylpyrimidine (DMAP) and its 6-ethyl analogue, DAEP.[65]

Biological Activity and Discussion

Compounds **3a** and **3b** were evaluated as inhibitors of *L. casei*, *E. coli*, rat, and human TS (Table 2) along with LY231514, ZD1694, and PDDF. For *L. casei* TS, compound **3a** was similar in potency to ZD1694 and 4.5-fold greater than LY231514, which, as mentioned above, is currently in phase III clinical trials as an antitumor agent. A comparison of the inhibitory potency of **3a** against *E.coli* TS indicates a significant difference between **3a** and LY231514. Compound **3a** was 100-fold greater than LY231514 in potency, although it was 10-fold less active than PDDF. Against rat, *L. casei*, and human TS, compound **3a** had IC_{50}'s of 2, 9, and 1 μM, respectively. Interestingly, compound **3b** was more active than **3a** and LY231514 against *L. casei* TS (IC_{50} = 0.31 μM).

Compounds **3a** and **3b** were also evaluated as inhibitors of *L. casei*, *E. coli*, *T. gondii*, *P. carinii*, and human DHFR (Table 3) compared to LY231514, MTX, and trimethoprim (TMP). Compound **3a** showed significant inhibitory activity ($IC_{50} = 2.4 \times 10^{-8}$ M) and was 10000-fold more potent than LY231514 against *L. casei* DHFR. Further, compound **3a** retained activities against *E. coli*, *T. gondii*, *P. carinii*, and human DHFR. Although compound **3a** was less potent than MTX in most cases, it was more than 100-fold more potent against *E. coli* and 10-fold more potent against human DHFR than LY231514. In contrast, compound **3b** was inactive against *L. casei*, *E. coli*, *T. gondii*, *P. carinii*, and human DHFR, indicating that the N7-benzyl moiety is not tolerated by DHFR.

The activities of **3a** and **3b** were compared to MTX as inhibitors of the growth of CCRF-CEM human leukemia and FaDu squamous cell carcinoma of the head and neck cell lines during continuous exposure in vitro (Table 4). Both parental cell lines were similarly sensitive to MTX under these conditions. Compound **3a** was as active (CCRF-CEM) and twice as active (FaDu) compared to MTX. Compound **3b** was inactive against both cell lines at the highest concentration tested; higher concentrations could not be tested because of vehicle (DMSO) toxicity.

To define the mechanism of action, compound **3a** was evaluated as a growth inhibitor of three CCRF-CEM sublines with defined MTX-resistance mechanisms (Table 5). A subline with increased DHFR expression, R1, is 48-fold resistant to MTX but only 13-fold cross-resistant to **3a**. A subline with decreased MTX uptake, R2, is 147-fold resistant to MTX but only 46-fold cross-resistant to **3a**. The subline with diminished ability to polyglutamylate MTX, R30dm, is not MTX-resistant in continuous exposure (resistance is only seen in intermittent exposure) because nonpolyglutamylated MTX is a tight-binding DHFR inhibitor and transport is sufficient to maintain drug in excess of DHFR. R30dm displays only 1.5-fold cross-resistance to **3a** in continuous exposure; the slope of its growth inhibition versus

Table 3. Inhibitory Concentrations against Isolated DHFR

	IC_{50} (M)				
compd	*L. casei*	*E. coli*[a]	*T. gondii*[b]	*P. carinii*[c]	human[d]
3a	2.4×10^{-8}	1.8×10^{-6}	1.2×10^{-6}	1.2×10^{-6}	8.0×10^{-7}
3b	$>1.9 \times 10^{-5}$	$>1.9 \times 10^{-5}$	$>1.9 \times 10^{-5}$	$>1.9 \times 10^{-5}$	$>1.9 \times 10^{-5}$
LY231514[e]	2.3×10^{-4}	2.3×10^{-4}	1.4×10^{-6}	2.3×10^{-6}	6.6×10^{-6}
MTX	4.4×10^{-8}	6.0×10^{-9}	2.2×10^{-8}	1.1×10^{-9}	2.2×10^{-8}
TMP	3.5×10^{-7}	2.0×10^{-8}	3.4×10^{-6}	1.5×10^{-5}	3.4×10^{-4}

[a] Kindly provided by Dr. R. L. Blakley, St. Jude Children's Research Hospital, Memphis, TN. [b] Kindly provided by Dr. D. V. Santi, University of California, San Francisco, CA. [c] Kindly provided by Dr. D. Borhanl, Southern Research Institute, Birmingham, AL. [d] Kindly provided by Dr. J. H. Freisheim, Medical College of Ohio, Toledo, OH. [e] Kindly provided by Dr. Chuan Shih, Eli Lilly & Co., Indianapolis, IN.

Table 4. Inhibition of Growth of CCRF-CEM Human Leukemia and FaDu Head and Neck Squamous Cell Carcinoma Cell Lines by MTX and **3a** in Continuous Exposure[a]

	EC_{50} (nM)	
drug	CCRF-CEM	FaDu
MTX	13.8 ± 1.6	14.5 ± 0.5
3a	12.5 ± 2.1 (n = 4)	7.0 ± 0 (n = 2)
3b	>10000[b] (n = 2)	>20000 (n = 2)

[a] Growth inhibition was assayed as described in the Experimental Section. Values presented are average ± SD if $n \geq 3$ and average ± range for $n = 2$. [b] No growth inhibition at 10 μM in two separate experiments; in one of these, 20 μM had a minor effect.

concentration curve against R30dm was also slightly shallower than that of MTX, and a 2.1-fold of **3a** was required to achieve 90% growth inhibition (data not shown).

Metabolite protection of growth inhibition was carried out to further define the mechanism of **3a**. FaDu cells were fully protected (data not shown) against growth inhibition by MTX (EC_{95}) and **3a** (EC_{95}) by the simultaneous presence of leucovorin (LV) at ≥0.1 μM. Protection by the purine hypoxanthine (Hx) and by thymidine (TdR) was also assessed (Table 6). At an EC_{95} MTX concentration, Hx alone or TdR alone protected to a low degree, but full protection required both Hx and TdR. At an EC_{95} level of **3a**, Hx alone offered no protection, while TdR alone was nearly fully protective; the combination of Hx and TdR consistently offered a slightly higher level of protection than TdR alone.

Protection of CCRF-CEM and R30dm cells by Hx and TdR was also assessed (Table 6); in this case a specific inhibitor of TS (ZD1694)[66] was also included in the evaluation. Parental CCRF-CEM required both Hx and TdR to be fully protected from MTX, similar to FaDu, whereas TdR alone was capable of protecting against ZD1694. CCRF-CEM cells were not protected against **3a** by Hx alone, whereas TdR gave substantial protection; a higher degree of protection was achieved with both Hx and TdR. A similar pattern of protection against all three drugs was observed with the polyglutamylation-deficient R30dm subline except that with **3a**, the requirement for both Hx and TdR was more striking.

Compound **3a** is a 4-CH_3 analogue of the multitargeted antifolate (MTA; LY231514) and its *N*-benzyl congener **3b**. Compound **3a** is as potent or more potent than MTX as a growth inhibitor of cell lines of two tumor types (Table 4). Growth inhibition data for CCRF-CEM cells with LY231514[67] show that it is 6-fold less potent than MTX in continuous exposure. Thus, although LY231514 was not directly compared with **3a** in our studies, it appears that the 4-CH_3 substitution is beneficial in terms of potency. Substitution at the N7 by a benzyl group is detrimental to the growth inhibitory potency of this class of analogues.

The cross-resistance pattern of the CCRF-CEM sublines to **3a** offers clues regarding the mechanism of action of this agent. Sublines with increased DHFR levels or decreased activity of the reduced folate/MTX carrier (RFC) are cross-resistant to this agent. This suggests that DHFR is a target despite the lack of a classical 2,4-diamino structure consistent with the design premise that the pyrrole nitrogen mimics the 4-amino moiety of the 2,4-diaminopyrimidine. Further, the analogue **3a** can be transported by the RFC. In both

Table 5. Growth Inhibition of Parental CCRF-CEM and Sublines with Single, Defined Mechanisms of MTX Resistance during Continuous (0−120 h) Exposure to MTX, **3a**, and **3b**[a]

	EC_{50} (nM)			
drug	CCRF-CEM	R1[b] (↑DHFR)	R2[c] (↓uptake)	R30dm[d] (↓Glu_n)
MTX	13.8 ± 1.6 (n = 4)	660 ± 40 (n = 2)	2030 ± 430 (n = 2)	15.5 ± 0.5 (n = 2)
3a	12.5 ± 2.1 (n = 4)	158 ± 8 (n = 2)	575 ± 25 (n = 2)	18.5 ± 0.5 (n = 2)
3b	>10000 (n = 2)	nd	nd	>20000[e]

[a] Average values are presented ± range for $n = 2$ and ± SD for $n \geq 3$; nd = not determined. [b] CCRF-CEM subline resistant to MTX solely as a result of a 20-fold increase in wild-type DHFR protein and activity. [c] CCRF-CEM subline resistant as a result of decreased uptake of MTX. [d] CCRF-CEM subline resistant to MTX solely as a result of decreased polyglutamylation; this cell line has 1% of the FPGS specific activity (measured with MTX as the foltate substrate) of parental CCRF-CEM. [e] Value was determined only once.

Table 6. Protection of Human Cells by Purine and/or Pyrimidine Metabolites from Growth Inhibition Induced by MTX, ZD1694 (Tomudex), or **3a**[a]

	relative growth			
drug	no addition	+Hx	+TdR	+(Hx + TdR)
		A. FaDu Cells		
MTX	4.5 ± 0.5	31 ± 1	11 ± 0	101 ± 0
3a	5.0 ± 0	5.0 ± 0	90.0 ± 0.5	96 ± 2
		B. CCRF-CEM Cells		
MTX	11.5 ± 0.5	18.5 ± 0.5	15 ± 0	91.5 ± 1.5
ZD1694	20.5 ± 1.5	24 ± 5	106.5 ± 1.5	107.5 ± 1.5
3a	13.5 ± 0.5	13 ± 0	88 ± 2	107.5 ± 0.5
		C. R30dm Cells		
MTX	15.5 ± 3.5	14.5 ± 0.5	12 ± 0	80 ± 1
ZD1694	15 ± 0	14.5 ± 0.5	95 ± 0	103.5 ± 2.5
3a	16 ± 0	16 ± 0	41.5 ± 3.5	86 ± 1

[a] Cells were exposed to drug concentrations previously shown to inhibit growth by 85−96%; metabolites were present simultaneously with drug. For FaDu cells: no addition, 50 μM Hx, 40 μM TdR, or a combination of Hx and TdR. For CCRF-CEM and R30dm cells: no addition, 10 μM Hx, 5 μM TdR, or a combination of Hx and TdR. Values are the average growth relative to a control culture treated only with metabolite (see Experimental Section); the error is the range of the two values used to determine the average. Each experiment was repeated with comparable results.

Table 7. Activity of Folate Analogues as Substrates for Recombinant Human FPGS[a]

substrate	K_m (μM)	V_{max}, rel	V/K	n
aminopterin	4.8 ± 0.7	1	0.21 ± 0.04	4
3a	<1	0.17 ± 0.02	>0.17	2
3b	37 ± 2	0.65 ± 0	0.02 ± 0	2

[a] FPGS substrate activity was determined as described in the Experimental Section. Values presented are average ± SD if $n \geq 3$ and average ± range for $n = 2$. V_{max} values are calculated relative to aminopterin within the same experiment.

cases, however, the cells are less resistant to **3a** than to MTX. This could indicate that the drug is more efficiently transported and/or polyglutamylated than is MTX and the higher intracellular levels attained are able to inhibit DHFR. The low level of cross-resistance of the polyglutamylation-deficient cell line R30dm could suggest that polyglutamylation of this analogue is not required for potent target inhibition by **3a** or that the analogue is an extremely efficient FPGS substrate; from Table 6 the latter is clearly the case.

The metabolite protection experiments suggest that **3a**, similar to LY231514,[67] may inhibit more than one pathway in folate metabolism. In FaDu cells, the primary target appears to be thymidylate biosynthesis since TdR alone can almost fully protect against **3a**. In CCRF-CEM cells, although thymidylate synthesis appears most sensitive, there is a component of inhibition of purine synthesis as well. Since DHFR appears to be a target in CCRF-CEM cells (above), purine synthesis inhibition is probably indirect.

Since polyglutamylation can markedly enhance the binding properties of substrate and inhibitors to folate-dependent enzymes, the polyglutamates of **3a** may be responsible for the inhibition of DHFR and TS.[68] Both **3a** and **3b** were tested as substrates for human FPGS to determine if polyglutamylation may be part of their mechanism of action (Table 7). Compound **3a** was an excellent FPGS substrate; although its V_{max} was relatively low, its very low K_m value (below the limit of detection of the assay) compensated for this deficiency. Despite the bulky benzyl substituent at N7, compound **3b** was also an FPGS substrate although its high K_m made it a relatively poor one, similar to MTX.[68]

Compound **3a** was selected by the National Cancer Institute[69] for evaluation as an antitumor agent in the preclinical in vitro screening program. The ability of **3a** to inhibit the growth of different tumor cell lines was measured as GI_{50} values, the concentration required to inhibit the growth of tumor cells in culture by 50% as compared to a control. Compound **3a** displayed potent antitumor activity with IC_{50} values in the 1.00×10^{-7} to 1.00×10^{-9} M range in eight cell lines. Data for compound **3a** are shown in Table 8.

Our synthetic strategy for this novel class of 2-amino-4-methyl-5-substituted pyrrolo[2,3-*d*]pyrimidine antifolates affords the key intermediate **10** in good yield, and this intermediate can be readily utilized for structure variation to afford a variety of 2-amino-4-methyl nonclassical and other classical antifolates, experiments of which are currently in progress.

Experimental Section

All evaporations were carried out in vacuo with a rotary evaporator. Analytical samples were dried in vacuo (0.2 mmHg) in an Abderhalden drying apparatus over P_2O_5 and refluxing ethanol. Thin-layer chromatography (TLC) was performed on silica gel plates with fluorescent indicator. Spots were visualized by UV light (254 and 365 nm). All analytical samples were homogeneous on TLC in at least two different solvent systems. Purification by column and flash chromatography was carried out using Merck silica gel 60 (200−400 mesh). The amount (weight) of silica gel for column chromatography was in the range of 50−100 times the amount (weight) of the crude compounds being separated. Columns were dry-packed unless specified otherwise. Solvent systems are reported as volume percent mixture. Melting points were determined on a Mel-Temp II melting point apparatus with a digital thermometer and are uncorrected. ^{1}H NMR spectra were recorded on a Bruker WH-300 (300 MHz) NMR spectrometer. The chemical shift (δ) values are reported as parts per million (ppm) relative to tetramethylsilane as internal standard; s = singlet, d = doublet, t = triplet, q = quartet, m = multiplet, br = broad peak, exch = protons exchangeable by addition of D_2O. Elemental analyses were performed by Atlantic Microlab, Inc., Norcross, GA. Elemental compositions were within ±0.4% of the calculated values. Fractional moles of water or organic solvents frequently found in some analytical samples of antifolates could not be removed despite 24 h of drying in vacuo and were confirmed, where possible, by their presence in the ^{1}H NMR spectrum. All solvents and chemicals were purchased from Aldrich Chemical Co. and Fisher Scientific and were used as received except anhydrous solvents which were freshly dried in the laboratory.

Table 8. Cytotoxicity Evaluation against Selected Tumor Cell Lines[69]

cell line	**3a**, GI_{50} (M)
leukemia	
MOLT-4	$<1.00 \times 10^{-8}$
non-small-cell lung cancer	
NCI−H226	6.14×10^{-8}
NCI−H460	$<1.00 \times 10^{-8}$
colon cancer	
HCC-2998	$<1.00 \times 10^{-8}$
HCT-116	7.11×10^{-6}
CNS cancer	
SF-539	$<1.00 \times 10^{-8}$
renal cancer	
ACHN	$<1.00 \times 10^{-8}$
breast cancer	
MCF7	1.69×10^{-7}

5-(2-Hydroxyethyl)-6-methyl-2-aminouracil (6). Method A. A mixture of 2-acetylbutyrolactone **(5)** (2.2 mL, 20 mmol) and guanidine carbonate (1.5 g, 20 mmol) was refluxed with absolute ethanol (20 mL) in the presence of triethylamine (5.5 mL, 40 mmol) for 1 h; the mixture became clear, then precipitated a pale yellow solid. The reaction was continued for 4 h. The precipitate was filtered, washed with ethanol and dried under vacuum to afford 1.16 g of **6** (69%) as a white solid.

Method B. Guanidine carbonate (0.75 g, 10 mmol) was added to a solution of NaOMe (0.45 g, 10 mmol) in absolute ethanol (50 mL). The mixture was stirred at 20−30 °C for 15 min, then 2-acetylbutyrolactone **(5)** (0.55 mL, 5 mmol) was added. The resulting mixture was refluxed for 16 h. The solvent was evaporated and 5 mL of water was added. The solution was acidified to pH 6−7 (using 1 N HCl) and filtered, the residue was washed with ethanol and dried under vacuum to afford 0.48 g of **6** (57%) as a white solid: TLC R_f 0.22 ($MeOH/CHCl_3$, 1:4); mp 263−264 °C dec; ^{1}H NMR (DMSO-d_6) δ 2.02 (s, 3 H, 4-CH_3), 2.43 (t, 2 H, J = 7.2 Hz, 7-CH_2), 3.30 (t, 2 H, J = 7.2 Hz, 8-CH_2), 4.51 (s, 1 H, OH, exch), 6.63 (s, 2 H, 2-NH_2, exch), 10.85 (s, 1 H, 3-NH, exch). Anal. ($C_7H_{11}N_3O_2$) C, H, N.

4-Chloro-5-(2-chloroethyl)-6-methylpyrimidine (7). A solution of **6** (1.69 g, 10 mmol) and phosphorus oxychloride (15 mL) was refluxed at 110 °C for 2 h. The excess $POCl_3$ was evaporated and the residue neutralized by 2% sodium carbonate solution to give 1.40 g (68%) of **7** as a white solid: TLC R_f 0.83 ($MeOH/CHCl_3$, 1:9); mp 195.5−197.5 °C; ^{1}H NMR (DMSO-

d_6) δ 2.34 (s, 3 H, 4-CH_3), 3.01 (t, 2 H, J = 3.6 Hz, 7-CH_2), 3.72 (t, 2 H, J = 3.6 Hz, 8-CH_2), 6.91 (s, 2 H, 2-NH_2, exch). Anal. ($C_7H_9N_3Cl_2$) C, H, N, Cl.

2-Amino-4-methyl-7-(*N*-benzyl)piperidinyl[2,3-*d*]pyrimidine (8). Compound **7** (10 g, 50 mmol) was dissolved in 120 mL of *n*-BuOH. To this solution were added benzylamine (6.5 mL, 60 mmol) and 15 mL of triethylamine. The mixture was refluxed at 110 °C for 3 days. The solvent was removed by evaporation. To this solution were added methanol (50 mL) and silica gel (10 g) and the solvent evaporated. The silica gel plug obtained was loaded onto a silica gel column and eluted with 9:1 ethyl acetate−triethylamine. The fractions containing the product (TLC) were pooled and the solvent evaporated to afford 5.98 g of **8** (50%) as a white solid: TLC R_f 0.22 (ethyl acetate/triethylamine/petroleum ether, 5:1:3); mp 172.5−174.5 °C; ^{1}H NMR (DMSO-d_6) δ 1.97 (s, 3 H, 4-CH_3), 2.77 (t, 2 H, J = 8.7 Hz, 5-CH_2), 3.35 (t, 2 H, J = 8.7 Hz, 6-CH_2), 4.47 (s, 2 H, C$H_2C_6H_5$), 5.86 (s, 2 H, 2-NH_2), 7.23−7.33 (m, 5 H, C_6H_5). Anal. ($C_{14}H_{16}N_4$·0.2CH_3OH) C, H, N.

2-Amino-4-methyl-7-(*N*-benzyl)pyrrolo[2,3-*d*]pyrimidine (9). Compound **8** (3.30 g, 14 mmol) was dissolved in 100 mL of 1,4-dioxane and 6.0 g of MnO_2 was added to the solution. The reaction mixture was refluxed in an oil bath at 110−120 °C for 24 h, filtered and to the filtrate was added 10 g of silica gel and the solvent evaporated. The silica gel plug obtained was loaded onto silica gel column and eluted with 5:1:3 ethyl acetate−triethylamine−petroleum ether. The fractions containing the product (TLC) were pooled and the solvent evaporated to afford 1.49 g of **9** (45%) as a pale yellow solid: TLC R_f 0.44 (ethyl acetate/triethylamine/petroleum ether, 5:1:3); mp 124−126.5 °C; ^{1}H NMR (DMSO-d_6) δ 2.39 (s, 3 H, 4-CH_3), 5.20 (s, 2 H, C$H_2C_6H_5$), 6.10 (s, 2 H, 2-NH_2, exch), 6.36 (d, 1 H, J = 3.6 Hz, 5-H), 7.01 (d, 1 H, J = 3.6 Hz, 6-H), 7.10−7.27 (m, 5 H, C_6H_5). Anal. ($C_{14}H_{14}N_4$) C, H, N.

2-Amino-4-methylpyrrolo[2,3-*d*]pyrimidine (10). To a round-bottomed flask was added **9** (1.26 g, 5 mmol) in 50 mL of liquid NH_3, followed by the addition of 500 mg of sodium metal. The reaction was maintained at −78 °C, as a deep blue solution for 1.5 h and then quenched with NH_4Cl (0.80 g). The temperature was raised to room temperature and the liquid NH_3 allowed to evaporate. The residue was purified by column chromatography on silica gel eluting with 20:2:2:1 ethyl acetate−ethanol−acetone−water. The fractions containing the desired product (TLC) were pooled, and the solvent evaporated to afford 0.43 g of **10** (65%) as a yellow solid: TLC R_f 0.46 (ethyl acetate/ethanol/acetone/water, 20:2:2:1); mp 207−209 °C; ^{1}H NMR (DMSO-d_6) δ 2.40 (s, 3 H, CH_3), 5.93 (s, 2 H, 2-NH_2, exch), 6.30 (d, 1 H, J = 3.6 Hz, 5-H), 6.92 (d, 1 H, J = 3.6 Hz, 6-H), 11.01 (s, 1 H, 7-NH, exch). Anal. ($C_7H_8N_4$) C, H, N.

2-Pivaloylamino-4-methylpyrrolo[2,3-*d*]pyrimidine (11). To a 50-mL round-bottomed flask was added **10** (0.82 g, 5 mmol) in 12 mL of anhydrous pyridine. To this solution was added pivaloyl chloride (2.2 mL, 17.5 mmol). The reaction was heated to reflux for 2 h under nitrogen. The volatiles were removed in vacuo, and the residue dissolved in 9 mL of methanol and cooled in an ice bath. To the stirred solution was added 15 mL of 10% ammonium hydroxide and the resulting precipitate was filtered, washed with water, ether and dried under vacuum to afford 0.84 g of **11** (65%) as a tan solid: TLC R_f 0.69 (ethyl acetate/ethanol/acetone/water, 20:2:2:1); mp 204−207 °C; ^{1}H NMR (DMSO-d_6) δ 1.22 (s, 9 H, CH_3), 2.60 (s, 3 H, 4-CH_3), 6.57 (d, 1 H, J = 3.6 Hz, 5-H), 7.35 (d, 1 H, J = 3.6 Hz, 6-H), 9.67 (s, 1 H, 2-N*H*Piv, exch), 11.83 (s, 1 H, NH, exch). Anal. ($C_{12}H_{16}N_4O$·0.5MeOH) C, H, N.

2-Pivaloylamino-4-methyl-5-iodopyrrolo[2,3-*d*]pyrimidine (12). To a 50-mL round-bottomed flask protected from light with aluminum foil were added **11** (0.75 g, 3.23 mmol) and *N*-iodosuccinimide (0.80 g, 3.55 mmol) dissolved in 15 mL of anhydrous THF. The reaction mixture was stirred under nitrogen for 8 h. The solvent was removed in vacuo, and the residue was dissolved in 150 mL of dichloromethane. The reaction mixture was washed with water, dried (Na_2SO_4) and concentrated in vacuo. The crude residue was then flash chromatographed on silica gel and eluted with 1:19 methanol−chloroform (v:v). The fractions containing the desired product (TLC) were pooled and evaporated to afford 0.60 g of **12** (52%) as a pale yellow solid: TLC R_f 0.32 (MeOH/$CHCl_3$, 1:19); mp 200−202 °C; ^{1}H NMR (DMSO-d_6) δ 1.22 (s 9 H, CH_3), 2.82 (s, 3 H, 4-CH_3), 7.61 (d, 1 H, J = 2.2 Hz, 6-H), 9.78 (s, 1 H, 2-N*H*Piv, exch), 12.26 (s, 1 H, 7-NH, exch). Anal. ($C_{12}H_{15}ON_4I$·0.5MeOH) C, H, N, I.

2-Pivaloylamino-4-methyl-5-trimethylsilylethynylpyrrolo[2,3-*d*]pyrimidine (13). To a 25-mL round-bottomed flask protected from light with aluminum foil were added **12** (72 mg, 0.2 mmol), copper(I) iodide (19 mg, 0.1 mmol), trimethylsilylacetylene (118 mg, 1.2 mmol), and tetrakis-(triphenylphosphine)palladium(0) (23 mg, 0.02 mmol) dissolved in 5 mL of anhydrous THF and 0.1 mL of triethylamine. The solution was stirred at room temperature overnight under nitrogen. The volatiles were removed in vacuo, and the residue dissolved in 20 mL of methylene chloride. The reaction mixture was washed with water, dried (Na_2SO_4) and concentrated in vacuo. The crude residue was then flash chromatographed on silica gel eluted with 1% MeOH/$CHCl_3$ by volume. The fractions containing the desired product (TLC) were pooled and evaporated to afford 30 mg (45.5%) of **13** as a tan solid: TLC R_f 0.43 (MeOH/$CHCl_3$, 1:19); ^{1}H NMR (DMSO-d_6) δ 0.23 (s, 9 H, CH_3), 1.22 (s, 9 H, CH_3), 2.77 (s, 3 H, 4-CH_3), 7.76 (s, 1 H, 6-H), 9.78 (s, 1 H, 2-N*H*Piv, exch), 12.26 (s, 1 H, 7-NH, exch).

2-Pivaloylamino-4-methyl-5-ethynylpyrrolo[2,3-*d*]pyrimidine (14). To a round-bottomed flask were added **13** (163 mg, 0.5 mmol) and 1 mL of tetrabutylammonium fluoride dissolved in 5 mL of THF. The reaction mixture was heated at 50 °C under nitrogen and stirred overnight. The reaction was then quenched by pouring it into 50 mL of chloroform and washed with water. The organic layer was separated, dried (Na_2SO_4) and concentrated in vacuo. The residue was then flash chromatographed and eluted with 1:19 MeOH−$CHCl_3$ (v:v). The fractions containing the desired product (TLC) were pooled and evaporated to afford 105 mg of **14** (98%) as a tan solid: TLC R_f 0.38 (MeOH/$CHCl_3$, 1:19); mp 200 °C dec; ^{1}H NMR (DMSO-d_6) δ 1.22 (s, 9 H, CH_3), 2.76 (s, 3 H, CH_3), 4.19 (s, 1 H, CH), 7.76 (d, 1 H, J = 2.2 Hz, 6-H), 9.79 (s, 1 H, 2-N*H*Piv, exch), 12.24 (s, 1 H, 7-NH, exch). Anal. ($C_{14}H_{16}N_4O$) C, H, N.

Diethyl *N*-{2-Pivaloylamino-4-methyl[(pyrrolo[2,3-*d*]-pyrimidin-5-yl)ethynyl]benzoyl}-L-glutamate (15). To a 25-mL round-bottomed flask protected from light with aluminum foil were added **14** (150 mg, 0.59 mmol), diethyl 4-iodobenzoyl-L-glutamate (281 mg, 0.65 mmol), tetrakis(triphenylphosphine)palladium(0) (71 mg, 0.059 mmol) and copper iodide (6 mg, 0.01 mmol) dissolved in 5 mL of anhydrous THF, followed by the addition of 0.1 mL of triethylamine. The resulting dark solution was stirred at room temperature under nitrogen for 28 h. Then 20 mL of methylene chloride was added to the solution and the reaction mixture was washed with water, dried (Na_2SO_4) and concentrated in vacuo. The crude residue was flash chromatographed on silica gel and eluted with 1:19 MeOH−$CHCl_3$ (v:v). The fractions containing the desired product (TLC) were pooled and evaporated to afford 140 mg (42.7%) of **15** as a tan solid: TLC R_f 0.44 (MeOH/$CHCl_3$, 1:19); mp 210−212 °C; ^{1}H NMR (DMSO-d_6) δ 1.19 (m, 6 H, $COOCH_2CH_3$), 2.10 (m, 2 H, $CH_2CH_2COOC_2H_5$), 2.45 (t, 2 H, J = 7.3 Hz, $CH_2CH_2COOC_2H_5$), 2.88 (s, 3 H, 4-CH_3), 4.09 (m, 4 H, $COOCH_2CH_3$), 4.45 (m, 1 H, CONHC*H*), 7.64 (d, 2 H, J = 8.2 Hz, C_6H_4), 7.88 (s, 1 H, 6-H), 7.93 (d, 2 H, J = 8.2 Hz, C_6H_4), 8.82 (d, 1 H, J = 7.4 Hz, CONH, exch), 9.81 (s, 1 H, 2-N*H*Piv, exch), 12.40 (s, 1 H, 7-NH, exch). Anal. ($C_{30}H_{35}N_5O_6$·0.5MeOH) C, H, N.

Diethyl *N*-{2-Pivaloylamino-4-methyl[(pyrrolo[2,3-*d*]-pyrimidin-5-yl)ethyl]benzoyl}-L-glutamate (16). To a Parr hydrogenation bottle was added **15** (90 mg, 0.16 mmol) dissolved in 15 mL of MeOH and 15 mL of methylene chloride, followed by the addition of 100 mg of 5% Pd/C. This mixture was hydrogenated at 50 psi for 18 h. After filtering and washing the catalyst thoroughly with methanol, the filtrate was concentrated in vacuo. The crude residue was then flash

chromatographed on silica gel and eluted with 1:19 MeOH−$CHCl_3$. The fractions containing the desired product (TLC) were pooled and evaporated to afford 70 mg (76%) of **16** as a pale yellow solid: TLC R_f 0.39 (MeOH/$CHCl_3$, 1:19); mp 146.5−148 °C; ^{1}H NMR (DMSO-d_6) δ 1.18 (m, 6 H, $COOCH_2CH_3$), 2.03 (m, 1 H, $CHHCH_2COOC_2H_5$), 2.09 (m, 1 H, $CHHCH_2COOC_2H_5$), 2.10 (t, 2 H, J = 7.3 Hz, $CH_2CH_2COOC_2H_5$), 2.69 (s, 3 H, 4-CH_3), 3.05 (m, 4 H, CH_2CH_2), 4.08 (m, 4 H, $COOCH_2CH_3$), 4.43 (m, 1 H, CONHC*H*), 7.08 (s, 1 H, 6-H), 7.35 (d, 2 H, J = 8.1 Hz, C_6H_4), 7.80 (d, 2 H, J = 8.1 Hz, C_6H_4), 8.65 (d, 1 H, J = 7.4 Hz, CONH, exch), 9.63 (s, 1 H, 2-N*H*Piv, exch), 11.55 (s, 1 H, 7-NH, exch). Anal. ($C_{30}H_{39}N_5O_6$) C, H, N.

***N*-{2-Amino-4-methyl[(pyrrolo[2,3-*d*]pyrimidin-5-yl)-ethyl]benzoyl}-L-glutamic Acid (3a).** To a round-bottomed flask was added **16** (60 mg, 0.11 mmol) suspended in 1 mL of 1.0 N NaOH. The reaction mixture was stirred at 50 °C for 3 days. The resulting solution was acidified with 1.0 N HCl to pH 3−4, and the precipitated mixture was cooled in an ice bath, filtered, washed with water, and dried in vacuo to give 32 mg (71%) of **3a** as a white solid: mp 270 °C dec; ^{1}H NMR (DMSO-d_6) δ 1.95 (m, 1 H, $CHHCH_2COOC_2H_5$), 2.10 (m, 1 H, $CHHCH_2COOC_2H_5$), 2.35 (t, 2 H, J = 7.2 Hz, CH_2CH_2COOH), 2.68 (s, 3 H, 4-CH_3), 2.98 (m, 4 H, CH_2CH_2), 4.39 (m, 1 H, CONHC*H*), 6.94 (br, 3 H, 2-NH_2 & 6-H), 7.35 (d, 2 H, J = 8.0 Hz, C_6H_4), 7.82 (d, 2 H, J = 8.0 Hz, C_6H_4), 8.55 (d, 1 H, J = 7.6 Hz, CONH, exch), 11.54 (s, 1 H, 7-NH, exch), 12.50 (br s, 2 H, COOH, exch). Anal. ($C_{21}H_{24}N_5O_5$) C, H, N.

2,2-Dipivaloylamino-4-methyl-7-(*N*-benzyl)pyrrolo[2,3-*d*]pyrimidine (17). Compound **9** (0.28 g, 1.18 mmol) was dissolved in 5 mL of dichloroethane; then trimethylacetyl chloride (0.20 mL, 2.36 mmol), DMAP (20 mg, 0.16 mmol) and triethylamine (0.40 mL) were added. The mixture was stirred overnight at 50 °C. The mixture was cooled, diluted with dichloromethane (20 mL), washed with brine (20 mL × 2), dried over Na_2SO_4 and concentrated in vacuo. To this solution were added methylene chloride (10 mL) and silica gel (5 mg) and the solvent evaporated. The silica gel plug obtained was loaded onto a silica gel column and eluted with 9:1 ethyl acetate−triethylamine. The fractions containing the product (TLC) were pooled and the solvent was evaporated to afford 0.38 g (79%) of **17** as a white solid: TLC R_f 0.47 (ethyl acetate/triethylamine/petroleum ether, 10:7:50); mp 116−117 °C; ^{1}H NMR (DMSO-d_6) δ 1.12 (s, 18 H, CH_3), 2.61 (s, 3 H, 4-CH_3), 5.43 (s, 2 H, $CH_2C_6H_5$), 6.74 (d, 1 H, J = 3.6 Hz, 5-H), 7.10−7.29 (m, 5 H, C_6H_5), 7.65 (d, 1 H, J = 3.6 Hz, 6-H). Anal. ($C_{24}H_{30}N_4O_2\cdot0.3H_2O$) C, H, N.

2,2-Dipivaloylamino-4-methyl-5-iodo-7-(*N*-benzyl)pyrrolo[2,3-*d*]pyrimidine (18). To a 15-mL round-bottomed flask protected from light with alumimum foil was added **17** (0.36 g, 0.89 mmol) dissolved in 5 mL of anhydrous DMF, followed by the addition of *N*-iodosuccinimide (0.23 g, 0.90 mmol). The dark brown solution was stirred at room temperature under a nitrogen atmosphere overnight. The solvent was removed in vacuo and the residue was dissolved in dichloromethane (20 mL) which was washed with brine (20 mL × 2), dried over Na_2SO_4 and concentrated in vacuo. To this solution were added methylene chloride (10 mL) and silica gel (5 mg) and the solvent evaporated. The silica gel plug obtained was loaded onto a silica gel column and eluted with 9:1 ethyl acetate−triethylamine. The fractions containing the product (TLC) were pooled and the solvent evaporated to afford 0.31 g (72%) of **18** as a pale yellow solid: TLC R_f 0.58 (ethyl acetate/triethylamine/hexane, 1:1:6); mp 121.5−123 °C; ^{1}H NMR δ (DMSO-d_6) 1.16 (s, 18 H, CH_3), 2.85 (s, 3 H, 4-CH_3), 5.37 (s, 2 H, $CH_2C_6H_5$), 7.17−7.30 (m, 5 H, C_6H_5), 7.98 (d, 1 H, 6-H). Anal. ($C_{24}H_{29}N_4O_2I\cdot0.1C_6H_{14}$) C, H, N, I.

2,2-Dipivaloylamino-4-methyl-5-trimethylethynyl-7-(*N*-benzyl)pyrrolo[2,3-*d*]pyrimidine (19). To a 25-mL round-bottomed flask protected from light with aluminum foil were added **18** (106 mg, 0.2 mmol), copper(I) iodide (8 mg, 0.4 mmol), trimethylsilylacetylene (58.8 mg, 0.6 mmol), and tetrakis-(triphenylphosphine)palladium(0) (23 mg, 0.02 mmol) dissolved in 4 mL of anhydrous THF and 0.1 mL of triethylamine. The solution was stirred at room temperature overnight under nitrogen. The volatiles were removed in vacuo, and the residue dissolved in 20 mL of methylene chloride. The reaction mixture was washed with water, dried (Na_2SO_4) and concentrated in vacuo. The crude residue was then flash chromatographed on silica gel eluted with 1:1:15 ethyl acetate−triethylamine−hexane. The fractions containing the desired product (TLC) were pooled and evaporated to afford 90 mg (91%) of **19** as a tan solid: TLC R_f 0.65 (ethyl acetate/triethylamine/hexane, 1:1:7); mp 174−176 °C; ^{1}H NMR (DMSO-d_6) δ 0.24 (s, 9 H, CH_3), 1.22 (s, 18 H, CH_3), 2.80 (s, 3 H, CH_3), 5.35 (s, 2 H, $CH_2C_6H_5$), 7.16−7.30 (m, 5 H, C_6H_5), 8.11 (s, 1 H, 6-H).

2-Pivaloylamino-4-methyl-5-ethynyl-7-(*N*-benzyl)pyrrolo[2,3-*d*]pyrimidine (20). To a round-bottomed flask were added **19** (584 mg, 1.18 mmol) and 1 mL of tetrabutylammonium fluoride dissolved in 5 mL of THF. The reaction mixture was heated at 50 °C under nitrogen and stirred overnight. The reaction was then quenched by pouring it into 50 mL of chloroform and washed with water. The organic layer was separated, dried (Na_2SO_4) and concentrated in vacuo. The residue was then flash chromatographed and eluted with 1:1:10 ethyl acetate−triethylamine−hexane. The fractions containing the desired product (TLC) were pooled and evaporated to afford 339 mg of **20** (92%) as a pale yellow solid: TLC R_f 0.41 (ethyl acetate/triethylamine/hexane, 1:1:3); mp 193−195 °C; ^{1}H NMR (DMSO-d_6) δ 1.23 (s, 9 H, CH_3), 2.76 (s, 3 H, CH_3), 4.25 (s, 1 H, CH), 5.36 (s, 2 H, CH_2Ph), 7.27−7.33 (m, 5 H, C_6H_5), 7.88 (d, 1 H, 6-H), 9.90 (s, 1 H, 2-N*H*Piv, exch). Anal. ($C_{21}H_{22}N_4O$) C, H, N.

Diethyl *N*-{2-Pivaloylamino-4-methyl[(pyrrolo[2,3-*d*]-pyrimidin-5-yl)ethynyl-7-(*N*-benzyl)]benzoyl}-L-glutamate (21). To a 25-mL round-bottomed flask protected from light with aluminum foil were added **20** (173 mg, 0.50 mmol), diethyl 4-iodobenzoyl-L-glutamate (260 mg, 0.60 mmol), tetrakis(triphenylphosphine)palladium(0) (60 mg, 0.05 mmol) and copper iodide (6 mg, 0.01 mmol) dissolved in 5 mL of anhydrous THF, followed by the addition of 0.1 mL of triethylamine. The resulting dark solution was stirred at room temperature under a nitrogen atmosphere for 24 h. Then 20 mL of methylene chloride was added to the solution and the reaction mixture was washed with water, dried (Na_2SO_4) and concentrated in vacuo. The crude residue was flash chromatographed on silica gel and eluted with 1:1:3 ethyl acetate−triethylamine−hexane. The fractions containing the desired product (TLC) were pooled and evaporated to afford 277 mg (85%) of **21** as a yellow solid: TLC R_f 0.44 (ethyl acetate/triethylamine/hexane, 1:1:1); mp 76−79 °C; ^{1}H NMR (DMSO-d_6) δ 0.87−1.25 (m, 15 H, CH_3), 1.76−2.50 (m, 4 H, CH_2CH_2), 2.88 (s, 3 H, 4-CH_3), 4.04 (t, 2 H, J = 7.2 Hz, OCH_2CH_3), 4.15 (t, 2 H, J = 7.2 Hz, OCH_2CH_3), 4.45 (m, 1 H, CONHC*H*), 5.41 (s, 2 H, $CH_2C_6H_5$), 7.27−7.36 (m, 5 H, C_6H_5), 7.63 (d, 2 H, J = 10.8 Hz, C_6H_4), 7.91 (d, 2 H, J = 10.8 Hz, C_6H_4), 8.11 (s, 1 H, 6-H), 8.84 (d, 1 H, J = 7.2 Hz, CONH, exch), 9.95 (s, 1 H, 2-N*H*Piv, exch). Anal. ($C_{37}H_{41}N_5O_6$) C, H, N.

Diethyl *N*-{2-Pivaloylamino-4-methyl[(pyrrolo[2,3-*d*]-pyrimidin-5-yl)ethyl-7-(*N*-benzyl)]benzoyl}-L-glutamate (22). To a Parr hydrogenation bottle was added **21** (240 mg, 0.37 mmol) dissolved in 15 mL of MeOH and 15 mL of methylene chloride, followed by the addition of 100 mg of 5% Pd/C. This mixture was hydrogenated at 50 psi for 18 h. After filtering and washing the catalyst thoroughly with methanol, the filtrate was concentrated in vacuo. The crude residue was then flash chromatographed on silica gel and eluted with 1:1:1 ethyl acetate−triethylamine−hexane. The fractions containing the desired product (TLC) were pooled and evaporated to afford 152 mg (63%) of **22** as a pale yellow sticky oil: TLC R_f 0.46 (ethyl acetate/triethylamine/hexane, 5:1:3); ^{1}H NMR (DMSO-d_6) δ 1.14−1.23 (m, 15 H, CH_3), 2.00−2.50 (m, 4 H, CH_2CH_2), 2.71 (s, 3 H, 4-CH_3), 2.99−3.10 (m, 4 H, CH_2CH_2), 4.01−4.14 (m, 4 H, OCH_2CH_3), 4.43 (m, 1 H, CONHC*H*), 5.31 (s, 2 H, $CH_2C_6H_5$), 7.13−7.32 (m, 8 H, C_6H_5, C_6H_4 & 6-H), 7.78 (d, 2 H, J = 10.8 Hz, C_6H_4), 8.64 (d, 1 H, J = 7.2 Hz, CONH, exch), 9.72 (s, 1 H, 2-N*H*Piv, exch). Anal. ($C_{37}H_{45}N_5O_6$) C, H, N.

***N*-{2-Amino-4-methyl[(pyrrolo[2,3-*d*]pyrimidin-5-yl)-ethyl-7-(*N*-benzyl)]benzoyl}-L-glutamic Acid (3b).** To a

round-bottomed flask was added **22** (110 mg, 0.18 mmol) suspended in 5 mL of MeOH and 1 mL of 1.0 N NaOH. The reaction mixture was stirred at 50 °C for 3 days. The resulting solution was acidified with 1.0 N HCl to pH 3−4, and the precipitated mixture was cooled in an ice bath, filtered, washed with water, and dried in vacuo to give 58 mg (67%) of **3b** as a white solid: mp 165−168 °C; ^{1}H NMR (DMSO-d_6) δ 1.95−2.37 (m, 4 H, CH_2CH_2), 2.55 (s, 3 H, 4-CH_3), 2.98 (m, 4 H, CH_2-CH_2), 4.39 (m, 1 H, CONHC*H*), 5.17 (s, 2 H, C$H_2C_6H_5$), 6.89 (s, 1 H, 6-H), 7.07−7.81 (m, C_6H_5 & C_6H_4), 8.54 (d, 1 H, NH, exch), 12.50 (br s, 2 H, COOH, exch). Anal. ($C_{28}H_{30}N_5O_5\cdot H_2O$) C, H, N.

Drugs. Solutions used in cell culture studies were standardized using extinction coefficients. Extinction coefficients were determined for **3a** (pH 1, λ_{max} 242 nm (43 500); pH 7, λ_{max} 238 nm (43 500); pH 13, λ_{max} 237 nm (44 400)). Extinction coefficients for MTX, a generous gift of Immunex (Seattle, WA), were from the literature.[70]

Cell Lines and Methods for Measuring Growth Inhibitory Potency. All cell lines were verified to be negative for *Mycoplasma* contamination using the GenProbe test kit. The human T-lymphoblastic leukemia cell line CCRF-CEM[71] and its MTX-resistant sublines R1,[72] R2,[73] and R30dm[74] were cultured as described.[74] R1 expresses 20-fold elevated levels of DHFR, the target enzyme of MTX. R2 has dramatically reduced MTX uptake. R30dm expresses 1% of the FPGS activity of CCRF-CEM and is resistant to short-term, but not continuous, MTX exposure; however, R30dm is generally cross-resistant in continuous exposure to antifolates requiring polyglutamylation to form potent inhibitors. The FaDu human head and neck squamous cell carcinoma cell line was propagated in RPMI 1640/10% fetal calf serum (FCS); however, growth inhibition was measured in medium containing 5% FCS[75] to minimize the levels of purine and pyrimidines introduced from FCS. Growth inhibition of all cell lines by continuous drug exposure was assayed as described.[74,75] Growth inhibitory potency of **3a** was tested after solubilization in DMSO. EC_{50} values were determined visually from plots of percent control growth versus the logarithm of drug concentration.

Protection against growth inhibition was assayed by including metabolites simultaneously with a concentration of drug previously determined to inhibit growth by 80−95%; the remainder of the assay was as described, except that the exposure time for CCRF-CEM and its sublines was reduced to 72 h to preclude metabolite depletion. The metabolites included were: LV (0.1−10 μM) or TdR (5 μM for CCRF-CEM and R30dm, 40 μM for FaDu) or Hx (10 μM for CCRF-CEM and R30dm, 50 μM for FaDu) or a combination of TdR and Hx at the same individual concentrations. In all studies with CCRF-CEM and R30dm, 20 M deoxycytidine was included in the growth media to prevent cell growth inhibition by TdR and the combination of Hx and TdR;[76] 20 μM deoxycytidine itself had no effect on cell growth. Growth inhibition was measured relative to the appropriate metabolite-treated control; metabolites caused <9% growth inhibition in the absence of drug, however.

Folylpolyglutamate Synthetase Assay. Recombinant human FPGS was purified from *E. coli* strain LM109 (λDE3) transformed with the expression plasmid pET3A-25;[77] the host and plasmid were generously supplied by Dr. Barry Shane, Department of Nutrition, University of California at Berkely. To increase sensitivity because of the low kinetic constants of **3a**, the standard assay[78] was modified to a 0.5-mL volume for all compounds tested. The monoglutamate forms of **3a** and **3b** were fully recovered under standard assay conditions; thus polyglutamate forms would also be quantitatively recovered.

Preparation of Recombinant *P. carinii* DHFR for X-ray Crystal Structure. Recombinant *P. carinii* DHFR was also produced for enzyme assays. The gene sequence was identical to that previously reported.[79] The expression system used pET8C, which employs the T7 RNA polymerase.[80] Host *E. coli* containing the appropriate plasmid construction was grown in Luria broth culture with 75 μg/mL kanamycin at 37 °C on a rotary shaker. The culture was transferred to fresh medium and OD_{590} was monitored. When the OD_{590} reached 0.4, the culture was shifted to 42 °C for 30 min to induce the gene for 7T RNA polymerase. Rifampin 200 μg/mL was added to suppress *E. coli* RNA polymerase. After 30 min, the culture was shifted back to 37 °C for 90 min. Cells were harvested by centrifugation, washed, and suspended in appropriate buffer containing protease inhibitors and 2-mercaptoethanol as described above. Bacterial cells were ruptured by sonication. The 100000*g* supernate containing recombinant *P. carinii* DHFR has been the standard enzyme used in the screen under contract NO1-AI-35171. Studies with [^{35}S]methionine incorporation have shown this preparation to contain predominantly one heavy band on autoradiography at a molecular weight corresponding to DHFR.

Recombinant *P. carinii* DHFR can also be purified from these 100000*g* supernates. We currently produce about 4 mg of material suitable for X-ray crystallography from each purification. The first step was an ammonium sulfate precipitation to yield a concentrated 45−90% cut which consistently contained about 72% of the original activity. This material was loaded onto a P-100 column equilibrated with 100 mM sodium phosphate buffer pH 7.4 containing 20 mM 2-mercaptoethanol and eluted with the same buffer. Most of the protein eluted in the void volume of the column, but DHFR activity eluted in a broad peak at about 1.3 times the void volume. Fractions containing significant DHFR activity were combined and loaded directly onto an affinity column.

The affinity column was prepared from folate-Sepharose (Sigma). The resin was poured into an appropriate sized column and washed sequentially with 100 mg/mL ascorbate, 5 mg/mL sodium metabisulfite, and 10 mM phosphate buffer pH 7 with 20 mM 2-mercaptoethanol (PME). This treatment reduces the folate on the column to dihydrofolate, the substrate for DHFR. After washing to remove all traces of sodium metabisulfite, the sample containing DHFR was slowly loaded onto the column. When the entire sample was loaded, the column was washed with PME until protein in the eluate became undetectable. Elution continued with stepwise washing of ca. 2 column volumes of PME containing 0.1 M NaCl, PME with 0.5 M NaCl, and PME with 1 M NaCl; these steps remove proteins nonspecifically adsorbed to the column. DHFR was eluted with PME containing 1 M NaCl and 3 mM folate. Activity of DHFR from affinity columns can be maintained with folate and with glycerol. These materials are used during the concentration steps that follow the affinity column. Glycerol was added to all samples, and they were frozen at −70 °C until aliquots were analyzed for protein content, DHFR activity, and purity by SDS−polyacrylamide gel electrophoresis (SDS−PAGE).

Crystallization and X-ray Data Collection. Recombinant *P. carinii* DHFR was cloned, isolated, and purified as described above. The protein was washed in a centricon-10 three times with 50 mM MES buffer at pH 6.0 in 100 mM KCl buffer and concentrated to 14.3 mg/mL. A novel thermal gradient technique[81] was used to carry out the crystallization screens with *P. carinii* DHFR. Crystallization of the *P. carinii* DHFR−**3a** complex was carried out by adding 10 μL of protein, 3 μL of MES/KCl buffer and 7 μL of 50% (w/v) PEG 2000 in 50 mM MES pH 6.0, 100 mM KCl and placing the mixture in microcentrifuge tubes for equilibration on a thermal gradient apparatus. Samples of *P. carinii* DHFR were also incubated overnight at 4 °C with NADPH and **3a**. The protein was washed to remove excess inhibitor and cofactor and concentrated to 9.8 mg/mL. This sample was set up with 50% (w/v) PEG 2000 with 50 mM MES buffer pH 6.0 and placed in the thermal gradient device. Crystals grew over several weeks time and are monoclinic, space group $P2_1$, and diffract to 2.0 Å resolution. The lattice constants for the ternary complex of *P. carinii* DHFR−NADPH−**3a** are a = 37.332, b = 43.231, c = 61.241 Å; β = 94.59°. Data were collected at room temperature on the best crystal available on a Rigaku RaxisIV imaging plate system and the data processed with DENZO.[82] The R_{merge} for 2σ data was 4.9% and the completeness of the

Table 9. Crystal Properties and Refinement Statistics for the pcDHFR−NADPH−**3a** Complex

lattice constants, Å	37.332, 43.231, 61.241; $\beta = 94.59°$
space group	$P2_1$
resolution range, Å	50.0−2.0
R_{merge}, %	4.9
completeness (2.1−2.0 Å)	99.4
reflections used	11919
R factor, %	22.3
R_{free}, %	29.7
protein atoms	1678
water molecules	95
Ramachanran, procheck %	87.0
B factor (protein average), Å^2	46.54
B factor (NADPH average), Å^2	44.75
B factor (**3a** average), Å^2	30.55
bonded main chain (rmsd)	0.966 target (1.5)
bonded side chain	0.694 (2.0)
angle main chain	1.81 (2.0)
angle side chain	1.236 (2.5)

data was 99% in the shell between 2 and 2.1 Å. The data for the ternary complex refined to 22.3% for data to 2.0 Å resolution are included in Table 9.

The structure was solved by molecular replacement methods with the program using the coordinates of *P. carinii* DHFR−NADPH−**1b**.[64] Inspection of the resulting difference electron density map using the program CHAIN[83] running on a Silicon Graphics Impact R10000 workstation revealed density for a ternary complex. The final cycles of refinement were carried out using the program X-PLOR.[84] The Ramachandran conformational parameters from the last cycle of refinement generated by PROCHECK[85] showed that more than 87% of the residues have the most favored conformation and none are in disallowed regions. Coordinates for this structure have been deposited with the Protein Data Bank (PDB code 1e26).

Acknowledgment. This work was supported, in part, by grants from the National Institutes of Health, AI41743 (A.G.), AI44661 (A.G.), CA43500 (J.J.M.), CA10914 (R.L.K.), and GM1670 (V.C. and S.F.Q.), and by Roswell Park Cancer Institute Core Grant CA16056 (J.J.M.). The authors thank Ms. Cynthia Russell and Mr. Gregory Nagel for performing the cell culture studies. V.C. thanks Dawn Rak for crystal growth and Walt Pangborn for data collection.

References

(1) (a) Presented in part at the 214th American Chemical Society National Meeting, Boston, MA, Aug 23−27, 1998; Abstr. MEDI 332. (b) Presented in part at the International Union of Crystallography Congress, Glasgow, Scotland, U.K., Aug 4−13, 1999.
(2) Jackson, R. C. In *Antifolate Drugs in Cancer Therapy*; Jackman, A. L., Ed.; Humana Press: Totowa, NJ, 1999; pp 1−12.
(3) Berman, E. M.; Werbel, L. M. The Renewed Potential for Folate Antagonists in Contemporary Cancer Chemotherapy. *J. Med. Chem.* **1991**, *34*, 479−485.
(4) Blakley, R. L. Eukaryotic Dihydrofolate Reductase. *Adv. Enzymol. Mol. Biol.* **1995**, *70*, 23−102.
(5) MacKenzie, R. E. Biogenesis and Interconversion of Substituted Tetrahydrofolates. In *Folates and Pterins Chemistry and Biochemistry*; Blakley, R. L., Benkovic, S. J., Eds.; Wiley: New York, 1984; Vol. I, pp 255−306.
(6) Carreras, C. W.; Santi, D. V. Catalytic Mechanism and Structure of Thymidylate Synthase. *Annu. Rev. Biochem.* **1995**, *64*, 721−762.
(7) Petero, G. J.; Kohne, C. H. Fluoropyrimidines as Antifolate Drugs. *Antifolate Drugs Cancer Ther.* **1999**, 101−145.
(8) Jackman, A. L.; Boyle, F. T.; Harrap, K. R. Tomudex (ZD1694): From Concept to Care, a Program in Rational Drug Discovery. *Invest. New Drug* **1996**, *14*, 305−316.
(9) Bertino, J. R.; Kamen, B.; Romanini, A. Folate Antagonists. In *Cancer Medicine*; Holland, J. F., Frei, E., Bast, R. C., Kufe, D. W., Morton, D. L., Weichselbaum, R. R., Eds.; Williams & Wilkins; Baltimore, MD, 1997; Vol. 1, pp 907−921.
(10) Takimoto, C. H. Antifolates in Clinical Development. *Semin. Oncol.* **1997**, *24*, S18-40−S18-51.
(11) Jodrell, D. I.; Bowman, A.; Rye, R.; Byrne, B.; Boddy, A.; Rafi, I.; Taylor, G. A.; Johnston, A. A Phase I Study of the Lipophilic Thymidylate Synthase Inhibitor Thymitac™ (Nolatrexed dihydrochloride) Given by 10-day Oral Administration. *Br. J. Cancer* **1999**, *79*, 915−920.
(12) Rosowsky, A. Chemistry and Biological Activity of Antifolates. In *Progress in Medicinal Chemistry*; Ellis, G. P., West, G. B., Eds.; Elsevier Science: New York, 1989; Vol. 26, pp 1−252.
(13) Gangjee, A.; Elzein, E.; Kothare, M.; Vasudevan, A. Classical and Nonclassical Antifolates as Potential Antitumor, Antipneumocystis and Antitoxoplasma Agents. *Curr. Pharm. Des.* **1996**, *2*, 263−280.
(14) Jones, T. R.; Calvert, A. H.; Jackman, A. L.; Brown, S. J.; Jones, M.; Harrap, K. R. A Potent Antitumor Quinazoline Inhibitor of Thymidylate Synthase: Synthesis, Biological Properties and Therapeutic Results in Mice. *Eur. J. Cancer* **1981**, *17*, 11−19.
(15) Kisliuk, R. L.; Gaumont, Y.; Kumar, P.; Coutta, M.; Nair, M. G.; Nanavati, N. T.; Kalman, T. I. The Effect of Polyglutamylation on the Inhibitory Activity of Folate Analogues. In *Proceedings of the Second Workshop on Folyl and Antifolyl Polyglutamates*; Goldman, I. D., Ed.; Praeger: New York, 1985; pp 319−328.
(16) Kisliuk, R. L.; Gaumont, Y.; Powers, J. F.; Thorndike, J.; Nair, M. G.; Piper, J. R. Synergistic Growth Inhibition by Combination of Antifolates. In *Evaluation of Folate Metabolism in Health and Disease*; Picciano, M. F., Stokstad, E. L. R., Gregory, J. F., III, Eds.; Alan R. Liss: New York, 1990; pp 79−89.
(17) Galivan, J.; Nimec, Z.; Rhee, M. S. Synergistic Growth Inhibition of Rat Hepatoma Cells Exposed in vitro to *N*-10-propargyl-5,8-Dideazafolate With Methotrexate or the Lipophilic Antifolates Trimetrexate or Metoprine. *Cancer Res.* **1988**, *47*, 5256−5260.
(18) Galivan, J.; Rhee, M. S.; Johnson, T. B.; Dilwith, R.; Nair, M. G.; Bunni, M.; Priest, D. G. The Role of Cellular Folates in the Enhancement of Activity of the Thymidylate Synthase Inhibitor 10-Propargyl-5,8-dideazafolate against Hepatoma Cells In Vitro by Inhibitors of Dihydrofolate Reductase. *J. Biol. Chem.* **1989**, *264*, 10685−10692.
(19) Gaumont, Y.; Kisliuk, R. L.; Emkey, R.; Piper, J. R.; Nair, M. G. Folate Enhancement of Antifolate Synergism in Human Lymphoma Cells. In *Chemistry and Biology of Pteridines*; Curtius, H. C., Blau, N., Ghisla, S., Eds.; W. deGruyter: Berlin, 1990; pp 1132−1136.
(20) Gaumont, Y.; Kisliuk, R. L.; Parsons, J. C.; Greco, W. R. Quanatitation of Folic Acid Enhancement of Antifolate Synergism. *Cancer Res.* **1992**, *52*, 2228−2235.
(21) Hynes, J. B.; Patil, S. A.; Tomčič, A.; Kumar, A.; Pathak, A.; Tan, X.; Xianqiang, L.; Ratnam, M.; Delcamp, T. J.; Freisheim, J. H. Inhibition of Murine Thymidylate Synthase and Human Dihydrofolate Reductase by 5,8-Dideaza Analogues of Folic Acid and Aminopterin. *J. Med. Chem.* **1988**, *31*, 449−454.
(22) Gangjee, A.; Devraj, R.; McGuire, J. J.; Kisliuk, R. L.; Queener, S. F.; Barrows, L. R. Classical and Nonclassical Furo[2,3-*d*]-pyrimidines as Novel Antifolates: Synthesis and Biological Activities. *J. Med. Chem.* **1994**, *37*, 1169−1176.
(23) Gangjee, A.; Devraj, R.; McGuire, J. J.; Kisliuk, R. L. Effect of Bridge Region Variation on Antifolate and Antitumor Activity of Classical 5-Substituted 2,4-Diminofuro[2,3-*d*]pyrimidines. *J. Med. Chem.* **1995**, *38*, 3798−3805.
(24) Calvert, H. MTA: Summary and Conclusions. *Semin. Oncol.* **1999**, *26* (Suppl. 6), 105−108.
(25) Tripos, Inc., 1699 S. Hanley Rd., St. Louis, MO 63144.
(26) Miwa, T.; Hitaka, T.; Akimoto, H. A.; Nomura, H. Novel Pyrrolo-[2,3-*d*]pyrimidine Antifolates: Synthesis and Antitumor Activities. *J. Med. Chem.* **1991**, *34*, 555−560.
(27) Kuyper, L. F.; Garvey, J. M.; Baccanari, D. P.; Champness, J. N.; Stammers, D. K.; Beddell, C. R. Pyrrolo[2,3-*d*]pyrimidines and Pyrido[2,3-*d*]pyrimidines as Conformationally Restricted Analogues of the Antibacterial Agent Trimethoprim. *Bioorg. Med. Chem.* **1996**, *4*, 593−602.
(28) Matthews, D. A.; Appelt, K.; Oatley, S. J.; Xuong, N. H. Crystal Structure of *Escherichia coli* Thymidylate Synthase Containing Bound 5-Fluoro-2′-Deoxyuridylate and 10-Propargyl-5,8-Dideazafolate. *J. Mol. Biol.* **1990**, *214*, 923−936.
(29) Rutenber, E. E.; Stroud, M. Binding of The Anticancer Drug ZD1694 to *E. coli* Thymidylate Synthase: Assessing Specificity and Affinity. *Structure* **1996**, *4*, 1317−1324.
(30) Webber, S. E.; Bleckman, T. D.; Attard, J.; Deal, J. G.; Kathardekar, V.; Welsh, K. M.; Webber, S.; Janson, C. A.; Matthews, D. A.; Smith, W. W.; Freer, S. T.; Jordan, S. R.; Bacquet, R. J. Howland, E. F.; Booth, C. L. J.; Ward, R. W.; Hermann, S. M.; White, J.; Morse, C. A.; Hilliard, J. A.; Bartlett, C. A. Design of Thymidylate Synthase Inhibitors Using Protein Crystal Structures: The Synthesis and Biological Evaluation of a Novel Class of 5-Substituted Quinazolinones. *J. Med. Chem.* **1993**, *36*, 733−746.
(31) Appelt, K.; Bacquet, R. J.; Bartlett, C. A.; Booth, C. L. J.; Freer, S. T.; Fuhry, M. M.; Gehring, M. R.; Herrmann, S. M.; Howland, E. F.; Janson, C. A.; Jones, T. R.; Kan, C.; Kathardekar, V.;

Lewis, K. K.; Marzoni, G. P.; Mattews, D. A.; Mohr, C.; Moomaw, E. W.; Morse, C. A.; Oatley, S. J.; Ogden, R. C.; Reddy, M. R.; Reich, S. H.; Schoettlin, W. S.; Smith, W. W.; Varney, M. D.; Villafranca, J. E.; Ward, R. W.; Webber, S.; Webber, S. E.; Welsh, K. M.; White, J. Design of Enzyme Inhibitors Using Iterative Protein Crystallographic Analysis. *J. Med. Chem*. **1991**, *34*, 1925−1934.

(32) Varney, M. D.; Marzoni, G. P.; Palmer, C. L.; Deal, J. G.; Webber, S.; Welsh, K. M.; Bacquet, R. J.; Bartlett, C. A.; Morse, C. A.; Booth, C. L. J.; Herrmann, S. M.; Howland, E. F.; Ward, R. W.; White, J. Crystal Structure-Based Design and Synthesis of Benz-[cd]indole-Containing Inhibitors of Thymidylate Synthase. *J. Med. Chem*. **1992**, *35*, 663−676.

(33) Reich, S. H.; Fuhry, M. M.; Nguyen, D.; Pino, M. J.; Welsh, K. M.; Webber, S.; Janson, C. A.; Jordan, S. R.; Matthews, D. A.; Smith, W. W.; Bartlett, C. A.; Booth, C. L. J.; Herrmann, S. M.; Howland, E. F.; Morse, C. A.; Ward, R. W.; White, J. Design and Synthesis of Novel 6,7-Imidazotetrahydroquinoline Inhibitors of Thymidylate Synthase Using Iterative Protein Crystal Structure Analysis. *J. Med. Chem*. **1992**, *35*, 847−858.

(34) Jackman, A. L.; Taylor, G. A.; Gibson, W.; Kimbell, R.; Brown, M.; Calvert, A. H.; Judson, I. R.; Hughes, L. R. ICI D1694, A Quinazoline Antifolate Thymidylate Synthase Inhibitor That is a Potent Inhibitor of L1210 Tumour Cell Growth In Vitro and In Vivo: A New Agent for Clinical Study. *Cancer Res*. **1991**, *51*, 5579−5586.

(35) Taylor, E. C.; Kuhnt, D.; Shih, C.; Rinzel, S. M.; Grindey, G. B.; Barredo, J.; Jannatipour, M.; Moran, R. A Dideazatetrahydrofolate Analogue Lacking a Chiral Center at C-6, *N*-[4-[2-(2-Amino-3,4-dihydro-4-oxo-7*H*-pyrrolo[2,3-*d*]pyrimidin-5-yl)ethyl]-benzoyl]-L-glutamate Acid, Is an Inhibitor of Thymidylate Synthase. *J. Med. Chem*. **1992**, *35*, 4450−4454.

(36) Jackman, A. L.; Gibson, W.; Stephems, T. C.; Boyle, F. T. Polyglutamylation of the Thymidylate Synthase (TS) Inhibitor, ICI D1694. *Proc. Am. Assoc. Cancer Res*. **1992**, *33*, 406.

(37) Sikora, E.; Jackman, A. L.; Newell, D. F.; Calvert, A. H. Formation and Retention and Biological Activity of N^{10}-Propargyl-5,8-dideazafolic Acid (CB 3717) Polyglutamations in L1210 Cells In Vitro. *Biochem. Pharmacol*. **1988**, *37*, 4047−4054.

(38) Jackman, A. L.; Newell, D. R.; Gibson, W.; Jodrell, D. I.; Taylor, G. A.; Bishop, J. A.; Hughes, L. R.; Calvert, A. H. The Biochemical Pharmacology of the Thymidylate Synthase Inhibitor 2-Desamino-2-methyl-N^{10}-propargyl-5,8-dideazafolic Acid (ICI 198583). *Biochem. Pharmacol*. **1991**, *41*, 1885−1895.

(39) Nair, M. G.; Abraham, A.; McGuire, J. J.; Kisliuk, R. L.; Galivan, J. Polyglutamylation as a Determinate of Cytotoxicity of Classical Folate Analogue Inhibitors of Thymidylate Synthase and Glycinamide Ribonucleotide Formyltransferase. *Cell. Pharmacol*. **1994**, *1*, 245−249.

(40) Bisset, G. M. F.; Pawelczak, K.; Jackman, A. L.; Calvert, A. H.; Hughes, L. R. Syntheses and Thymidylate Synthase Inhibitory Activity of the Poly-γ-glutamyl Conjugates of *N*-[5-[*N*-(3,4-Dihydro-2-methyl-4-oxoquinazolin-6-ylmethyl)-*N*-methylamino]-2-thenoyl]-L-glutamic Acid (ICI D1694) and other Quinazoline Antifolates. *J. Med. Chem*. **1992**, *35*, 859−866.

(41) Bisset, G. M. F.; Bavetsias, V.; Thornton, T. J.; Pawelczak, K.; Calvert, A. H.; Hughes, L. R.; Jackman, A. L. The Synthesis and Thymidylate Synthase Inhibitory Activity of L-γ-L-Linked Dipeptide and L-γ-Aminde Analogues of 2-Desamino-2-methyl-N^{10}-propargyl-5,8-dideazafolic Acid (ICI 198583). *J. Med. Chem*. **1994**, *37*, 3294−3302.

(42) Jackman, A. L.; Kelland, L. R.; Brown, M.; Gibson, W.; Kimbell, R.; Aherne, W.; Judson, I. R. ICI D1694 Resistant Cell Lines. *Proc. Am. Assoc. Cancer Res*. **1992**, *33*, 406.

(43) Barakat, R. R.; Li, W. W.; Lovelace, C.; Bertino, J. R. Intrinsic Resistance of Squamous Cell Carcinoma Cell Lines as a result of Decreased Accumulation of Intracellular Methotrexate Polyglutamates. *Gynecol. Oncol*. **1993**, *51*, 54−60.

(44) McCloskey, D. E.; McGuire, J. J.; Russell, C. A.; Rowan, B. G.; Bertino, J. R.; Pizzorno, G.; Mini, E. Decreased Folylpolyglutamate Synthetase Activity as a Mechanism of Methotrexate Resistance in CCRF−CEM Human Leukemia Sublines. *J. Biol. Chem*. **1991**, *266*, 6181−6187.

(45) Braakhuis, B. J.; Jansen, G.; Noordhius, P.; Kegel, A.; Peters, G. J. Importance of Pharmacodynamics in the In Vitro Antiproliferative Activity of the Antifolates Methotrexate and 10-EDAM against Head and Neck Squamous Cell Carcinoma. *Biochem. Pharmacol*. **1993**, *46*, 2155−2161.

(46) Akimoto, H.; Ootsu, K. Preparation of N-{[(pyrrolopyrimidinyl)-alkyl]benzoyl}glutamates and Analogues as Antitumor Agents. Eur. Pat. Appl. 91-300266 19910115.

(47) Taylor, E. C.; Liu, B. A Novel Synthetic Route to 7-Substituted Derivatives of the Antitumor Agent LY231514 (MTX). *Tetrahedron Lett*. **1999**, *40*, 5291−5294.

(48) Badawey, E. A. M. Synthesis and In Vitro Evaluation of Some New Pyrimidines and Related Condensed Ring Systems as Potential Anticancer Agents. *J. Heterocycl. Chem*. **1996**, *33*, 229−233.

(49) Taylor, E. C.; Pont, J. L.; Warner, J. C. Synthesis of 2-Amino-6,7-dihydrothieno[3′,2′:5,6]pyrido[2,3-*d*]pyrimidine-4-one. *J. Heterocycl. Chem*. **1988**, *25*, 1733−1735.

(50) Felix, A. M.; Heimer, E. P.; Lambros, T. J.; Tzougraki, C.; Meienhofer, J. Rapid Removal of Protecting Groups from Peptides by Catalytic Transfer Hydrogenation with 1,4-Cyclohexadiene. *J. Org. Chem*. **1978**, *43*, 4194−4196.

(51) Lee, M.; Ikeda, I.; Kawabe, T.; Mori, S.; Kanematsu, K. Enantioselective Total Synthesis of *cis*-Trikentrin B. *J. Org. Chem*. **1996**, *61*, 3406−3416.

(52) Ram, S.; Spicer, L. D. Rapid Debenzylation of N-benzylamino Derivatives to Amino-derivatives Using Ammonium Formate as Catalytic Hydrogen Transfer Agent. *Tetrahedron Lett*. **1987**, *28*, 515−516.

(53) Philips, K. D.; Horwitz, J. P. Nucleosides. XVII. Benzylation-debenzylation Studies on Nucleosides. *J. Org. Chem*. **1975**, *40*, 1856−1858.

(54) Other reports of the difficulty of debenzylating *N*-benzylpyrroles can be found in the literature: e.g., Lim, M.-I.; Klein, R. S.; Fox, J. J. A New Synthesis of Pyrrolo[3,2-*d*]pyrimidines ("9-Deazapurines") via 3-Amino-2-carboalkoxy Pyrroles. *J. Org. Chem*. **1979**, *44*, 3826−3829 and Schneller, S. W.; Luo, J.-K.; Hosmane, R. S. 6-Amino-1*H*-pyrrolo[3,2-*c*]pyridin-4(5*H*)-one (3,7-Dideaza-guanine). *Tetrahedron Lett*. **1980**, *21*, 3135−3138.

(55) Edstrom, E. D.; Wei, Y. Synthesis of a Novel Pyrrolo[2,3-*d*]-pyrimidine Alkaloid, Rigidin. *J. Org. Chem*. **1993**, *58*, 403−407.

(56) Miah, S.; Moody, C. J.; Richards, I. C.; Slawin, A. M. Z. Synthesis of the Marine Dibromooxoindoline Convolutamydine C. *J. Chem. Soc., Perkin Trans. 1* **1997**, *16*, 2405−2415.

(57) Hoops, G. C.; Park, J.; Garcia, G. A.; Townsend, L. B. The Synthesis and Determination of Acidic Ionization Constants of Certain 5-Substituted 2-Aminopyrrolo[2,3-*d*]pyrimidin-4-ones and Methylated Analogues. *J. Heterocycl. Chem*. **1996**, *33*, 767−778.

(58) Shih, C.; Gossett, L. S. The Synthesis of N-{2-Amino-4-substituted[(pyrrolo[2,3-*d*]-pyrimidin-5-yl)ethyl]benzoyl}-L-glutamate Acids as Antitumor Agents. *Heterocycles* **1993**, *36*, 825−841.

(59) Taylor, E. C.; Young, W. B.; Chaudhari, R.; Patel, H, H. Synthesis of a Regioisomer of N-{4-[2-(2-amino-4(3H)-oxo-7H-pyrrolo-[2,3-*d*]pyrimidin-5-yl)ethyl]benzoyl}-L-glutamic acid (LY231514), an Active Thymidylate Synthase Inhibitor and Antitumor Agent. *Heterocycles* **1993**, *36*, 1897−1908.

(60) Sonogashira, K.; Tohda, Y.; Hagihara, N. A Convenient Synthesis of Acetylenes: Catalytic Substitutions of Acetylenic Hydrogen with Bromoalkenes, Iodoarenes, and Bromopyridines. *Tetrahedron Lett*. **1975**, *50*, 4467−4470.

(61) Taylor, E. C.; Wong, G. S. K. Convergent and Efficient Palladium-effected Synthesis of 5,10-Dideaza-5,6,7,8-tetrahydrofolic Acid (DDATHF). *J. Org. Chem*. **1989**, *54*, 3618−3624.

(62) Ramzaeva, N.; Seela, F. 88. 7-Substituted 7-Deaza-2′-deoxyguanosines: Regioselective Halogenation of Pyrrolo[2,3-*d*]pyrimidine Nucleosides. *Helv. Chim. Acta* **1995**, *78*, 1083−1090.

(63) Cody, V.; Galitsky, N.; Luft, J. R.; Pangborn, W.; Gangjee, A.; Devraj, R.; Queener, S. F.; Blakley, R. L. Comparison of Ternary Complexes of *Pneumocystis carinii* and Wild-Type Human Dihydrofolate Reductase With a Novel Classical Antitumor Furo-[2,3-*d*]pyrimidine Antifolate. *Acta Crystallogr*. **1997**, *D53*, 638−649.

(64) Cody, V.; Galitsky, N.; Rak, D.; Luft, J. R.; Pangborn, W.; Queener, S. F. Ligand Induced Conformational Changes in the Crystal Structures of *Pneumocystis carinii* Dihydrofolate Reductase Compleses With Folate and NDAP$^+$. *Biochemistry* **1999**, *38*, 4303−4312.

(65) Cody, V.; Rak, D.; Pangborn, W. Structure Determination of Lipophilic 5-Adamantyl Diaminopyrimidine Anticancer Agents as Cofactor Ternary Complexes with Human and *Pneumocystis carinii* Dihydrofolate Reductase. American Crystallographic Association Meeting, May 1999; Abstr. PM14, p 92.

(66) Jackman, A. L.; Taylor, G. A.; Gibson, W.; Kimbell, R.; Brown, M.; Calvert, A. H.; Judson, I. R.; Hughes, L. R. ICI D1694, a Quinazoline Antifolate Thymidylate Synthase Inhibitor That Is a Potent Inhibitor of L1210 Tumor Cell Growth In Vitro and In Vivo: A New Agent for Clinical Study. *Cancer Res*. **1991**, *51*, 5579−5586.

(67) Shih, C.; Chen, V. J.; Gossett, L. S.; Gates, S. B.; MacKellar, W. C.; Habeck, L. L.; Shackelford, K. A.; Mendelsohn, L. G.; Soose, D. J.; Patel, V. F.; Andis, S. L.; Bewley, J. R.; Rayl, E. A.; Moroson, B. A.; Beardsley, G. P.; Kohler, W.; Ratnam, M.; Schultz, R. M. LY231514, a Pyrrolo[2,3-*d*]pyrimidine-based Antifolate That Inhibits Multiple Folate-requiring Enzyme. *Cancer Res*. **1997**, *57*, 1116−1123.

(68) McGuire, J. J.; Coward, J. K. Pteroylpolyglutamates: Biosynthesis, degradation and function. In *Folates and Pterins Chemistry and Biochemistry*; Blakley, R. L., Benkovic, S. J., Eds.; Wiley: New York, 1984; Vol. I, pp 135−190.

(69) We thank the Developmental Therapeutics Program of the National Cancer Institute for performing the in vitro anticancer evaluation.
(70) Blakley, R. L. *The Biochemistry of Folic Acid and Related Pteridines*; Elsevier North-Holland: Amsterdam, 1969; pp 92−94.
(71) Foley, G. F.; Lazarus, H.; Farber, S.; Uzman, B. G.; Boone, B. A.; McCarthy, R. E. Continuous Culture of Lymphoblasts from Peripheral Blood of a Child with Acute Leukemia. *Cancer* **1965**, *18*, 522−529.
(72) Mini, E.; Srimatkandada, S.; Medina, W. D.; Moroson, B. A.; Carman, M. D.; Bertino, J. R. Molecular and Karyological Analysis of Methotrexate-resistant and -sensitive Human Leukemic CCRF-CEM Cells. *Cancer Res*. **1985**, *45*, 317−325.
(73) Rosowsky, A.; Lazarus, H.; Yuan, G. C.; Beltz, W. R.; Mangini, L.; Abelson, H. T.; Modest, E. J.; Frei, E., III. Effects of Methotrexate Esters and Other Lipophilic Antifolates on Methotrexate-resistant Human Leukemic Lymphoblasts. *Biochem. Pharmacol*. **1980**, *29*, 648−652.
(74) McCloskey, D. E.; McGuire, J. J.; Russell, C. A.; Rowan, B. G.; Bertino, J. R.; Pizzorno, G.; Mini, E. Decreased Folypolyglutamate Synthetase Activity as a Mechanism of Methotrexate Resistance in CCRF-CEM Human Leukemia Sublines. *J. Biol. Chem*. **1991**, *266*, 6181−6187.
(75) McGuire, J. J.; Magee, K. J.; Russell, C. A.; Canestrari, J. M. Thymidylate Synthase as a Target for Growth Inhibition in Methotrexate-sensitive and -resistant Human Head and Cancer and Leukemia Cell Lines. *Oncol. Res*. **1997**, *9*, 139−147.
(76) Grindey, G. B.; Wang, M. C.; Kinahan, J. J. Thymidine Induced Perturbations in Ribonucleoside and Deoxyribonucleoside Triphosphate Pools in Human Leukemic CCRF-CEM Cells. *Mol. Pharmacol*. **1979**, *16*, 601−606.
(77) Chen, L.; Qi, H.; Korenberg, J.; Garrow, T. A.; Choi, Y. J.; Shane, B. Purification and Properties of Human Cytosolic Folylpolygamma-glutamate Synthetase and Organization, Localization,and Differential Splicing of Its Gene. *J. Biol. Chem*. **1996**, *271*, 13077−13087.
(78) McGuire, J. J.; Hsieh, P.; Coward, J. K.; Bertino, J. R. In Vitro Methotrexate Polyglutamate Synthesis by Rat Liver Folylpolyglutamate Synthstase and Its Inhibition by Bromosulfophthalein. *Adv. Exp. Biol. Med*. **1983**, *163*, 199−214.
(79) Edman, J. C.; Edman, U.; Cao, M.; Lundgren, B.; Kovacs, J. A.; Santi, D. V. Isolation and Expression of the *Pneumocystis carinii* Dihydrofolate Reductase Gene. *Proc. Natl. Acad. Sci. U.S.A*. **1989**, *86*, 8625−8629.
(80) Triglia, T.; Cowman, A. F. Primary Structure and Expression of the Dihydropteroate Synthetase Gene of *Plasmodium falciparum*. *Proc. Natl. Acad. Sci. U.S.A*. **1994**, *91*, 7149−7153.
(81) Luft, J. R.; Rak, D. M.; DeTitta, G. T. Microbatch Macromolecular Crystal Growth Techniques. *J. Crystal Growth* **1999**, *196*, 447−449, 450−455.
(82) Otwinowski, Z.; Minor, W. Processing of X-ray Diffraction Data Collected in Oscillation Mode. In *Methods in Enzymology*; Carter, C. W., Jr.; Sweet, R. M., Eds.; Academic Press: New York, 1997; Vol. 276, Part A, pp 307−326.
(83) Sack, J. S. CHAIN-A Crystallographic Modeling Program. *J. Mol. Graph*. **1988**, *6*, 224−225.
(84) Brunger, A. T. *X-PLOR*; Yale University Press: New Heaven and London, 1992.
(85) Laskowski, R. A.; MacArthur, M. W.; Moss, D. S.; Thornton, J. M. PROCHECK: A Program to Check the Stereochemical Quality of Protein Structure. *J. Appl. Crystallogr*. **1993**, *26*, 283−291.

JM000200L